mSystems | Environmental Microbiology | Research Article

Putative novel hydrogen- and iron-oxidizing sheath-producing Zetaproteobacteria thrive at the Fåvne deep-sea hydrothermal vent field

Petra Hribovšek,[1,2] Emily Olesin Denny,[1,3,4] Håkon Dahle,[1,3,4] Achim Mall,[1,3] Thomas Øfstegaard Viflot,[1,2] Chanakan Boonnawa,[1,2] Eoghan P. Reeves,[1,2] Ida Helene Steen,[1,3] Runar Stokke[1,3]

AUTHOR AFFILIATIONS See affiliation list on p. 20.

ABSTRACT Iron-oxidizing Zetaproteobacteria are well known to colonize deep-sea hydrothermal vent fields around the world where iron-rich fluids are discharged into oxic seawater. How inter-field and intra-field differences in geochemistry influence the diversity of Zetaproteobacteria, however, remains largely unknown. Here, we characterize Zetaproteobacteria phylogenomic diversity, metabolic potential, and morphologies of the iron oxides they form, with a focus on the recently discovered Fåvne vent field. Located along the Mohns ridge in the Arctic, this vent field is a unique study site with vent fluids containing both iron and hydrogen with thick iron microbial mats (Fe mats) covering porously venting high-temperature (227–267°C) black smoker chimneys. Through genome-resolved metagenomics, we demonstrate that Zetaproteobacteria, *Ghiorsea* spp., likely produce tubular iron oxide sheaths dominating the Fe mats at Fåvne, as observed via microscopy. With these structures, *Ghiorsea* may provide a surface area for members of other abundant taxa such as Campylobacterota, Gammaproteobacteria, and Alphaproteobacteria. Furthermore, *Ghiorsea* likely oxidizes both iron and hydrogen present in the fluids, with several *Ghiorsea* populations co-existing in the same niche. Homologs of Zetaproteobacteria Ni,Fe hydrogenases and iron oxidation gene *cyc2* were found in genomes of other community members, suggesting exchange of these genes could have happened in similar environments. Our study provides new insights into Zetaproteobacteria in hydrothermal vents, their diversity, energy metabolism and niche formation.

IMPORTANCE Knowledge on microbial iron oxidation is important for understanding the cycling of iron, carbon, nitrogen, nutrients, and metals. The current study yields important insights into the niche sharing, diversification, and Fe(III) oxyhydroxide morphology of *Ghiorsea*, an iron- and hydrogen-oxidizing Zetaproteobacteria representative belonging to Zetaproteobacteria operational taxonomic unit 9. The study proposes that *Ghiorsea* exhibits a more extensive morphology of Fe(III) oxyhydroxide than previously observed. Overall, the results increase our knowledge on potential drivers of Zetaproteobacteria diversity in iron microbial mats and can eventually be used to develop strategies for the cultivation of sheath-forming Zetaproteobacteria.

KEYWORDS Zetaproteobacteria, iron oxidation, hydrogen oxidation, hydrothermal vents, microbial mats, genome-resolved metagenomics

Chemolithoautotrophic iron-oxidizing bacteria (FeOB) are frequently observed at deep-sea hydrothermal vents associated with Fe(II)-rich fluids. At neutral pH, FeOB can obtain energy by oxidation of Fe(II) under microaerobic conditions, some can grow anaerobically using nitrate as terminal electron acceptor or they can be

Editor Michael S. Rappe, University of Hawaii at Manoa, Kaneohe, Hawaii, USA

Address correspondence to Petra Hribovšek, petra.hribovsek@uib.no, or Runar Stokke, runar.stokke@uib.no.

The authors declare no conflict of interest.

Received 20 June 2023
Accepted 2 October 2023
Published 3 November 2023

photoferrotrophs, while there are acidophilic FeOB inhabiting low pH environments (1). Fe-oxidizers influence biogeochemical cycling of iron and other elements through transforming the soluble Fe(II) to insoluble Fe(III), which often takes the form of Fe(III) oxyhydroxides. These Fe(III) oxyhydroxides have the ability to co-precipitate and adsorb carbon, nutrients, and heavy metals (1–6). FeOB can also play a role in corrosion (7, 8) and bioremediation of metal pollution and recovery of resources (9, 10). Seafloor hydrothermal fluids are typically rich in diverse electron donors such as hydrogen sulfide and methane but with variable hydrogen and Fe contents (11–14). The exact chemical composition of these fluids varies widely between and often within vent fields, depending on the hydrothermal system's geological setting, and exerts a strong influence on the microbial communities present (15–17).

FeOB are found in iron microbial mats (Fe mats) around the globe, such as at the Kama'ehuakanaloa (Lō'ihi) seamount (18–22), Vailulu'u seamount (23), Mid-Atlantic Ridge (24, 25), the Mariana region (26–31), Kermadec Arc (32), South Tonga Arc (33), Mid-Cayman Ridge (34), and Arctic Mid-Ocean Ridges (AMOR) (35–37). The dominant FeOB in these Fe mats are Zetaproteobacteria, first proposed as a class in 2007 (38) and collectively divided into operational taxonomic units specific to subgroups of Zetaproteobacteria (ZetaOTUs) (39). To obtain energy for CO_2 fixation, Zetaproteobacteria oxidize soluble Fe(II) under low oxygen conditions (40). Micrometer-scale structures composed largely of extracellular polymeric substances and precipitated Fe(III) oxyhydroxides are often formed as a result of their Fe metabolism. The morphology of Fe(III) hydroxides varies between types of Zetaproteobacteria. Some produce twisted stalks, others produce hollow tubular sheaths, bifurcating tubular structures or dreads (18, 20, 41–43). It has been hypothesized that these structures prevent the cells from becoming encrusted in Fe and that they keep the cells within the gradient of oxygen and Fe required for growth (20, 38). While stalk formation genes have recently been proposed (44, 45), the molecular mechanisms for formation of other structures are not well studied, and not all morphologies have a known isolated representative. Fe(III) oxyhydroxide sheaths in marine environments were found associated with Zetaproteobacteria (18); however, to date, no sheath-forming Zetaproteobacteria have been isolated nor have the Zetaproteobacteria responsible for sheath formation been identified and confirmed. Since sheaths and stalks make up the majority of Fe mats, stalk- and sheath-forming Zetaproteobacteria are recognized as ecosystem engineers that produce the structure of these mats, providing a suitable environment for other species (20).

Only a few FeOB belonging to the Zetaproteobacteria have been cultured, most of which are members of the genus *Mariprofundus* (38, 41, 46–49). The *cyc2* gene has been validated as the main gene involved in the Fe oxidation pathway of Zetaproteobacteria and other bacteria in near-neutral pH environments (31, 50–52). While most of Zetaproteobacteria are strict FeOB, it has been shown that *Ghiorsea bivora*, a ZetaOTU9 representative, can obtain energy from hydrogen oxidation by using hydrogen as either the sole electron donor or in combination with Fe(II) (53). The co-occurrence of Fe(II) and H_2 may play an important role in defining the niche of ZetaOTU9 (40). However, we have a limited understanding of the functioning of FeOB that also use H_2 and how this affects their diversity and ecology. In this paper, we contribute toward narrowing this knowledge gap.

At the recently discovered Fåvne deep-sea hydrothermal vent field located on the Mohns Ridge (54–56), dense Fe mats cover porous black smoker chimney surfaces at *in situ* temperatures of ~50°C (see Supplementary Material 4 at https://doi.org/10.5281/zenodo.8297777). The venting fluids at Fåvne contain both abundant dissolved H_2 and Fe(II) as energy sources, with measured concentrations (±10%) of 22 and 24 mmol/L, respectively, in the North Tower duplicate isobaric gas-tight (IGT) fluid samples (55). In contrast to lower temperature Fe mat systems where H_2 is below detection or absent (14), these levels at Fåvne instead are more characteristic of black smoker fluids at sites such as Rainbow, Logatchev, and Azhadze 1 and 2 (57). This geochemistry makes Fåvne a valuable study site to investigate FeOB that can use H_2 as an alternate electron

donor. Our genome-resolved metagenomics and microscopy study characterize Fåvne Fe mats as a deep-sea hydrothermal habitat formed using abundant byproducts of novel sheath-forming Fe-oxidizing Zetaproteobacteria that potentially also utilize H_2. The identification of sheath-producing *Ghiorsea* belonging to ZetaOTU9 extends previous knowledge on Fe(III) oxyhydroxide morphologies. In addition, our results suggest that hydrogen could be the main driver of diversity of Zetaproteobacteria interacting with vent fluids containing both Fe(II) and H_2, where flexible lithotrophic energy metabolism of *Ghiorsea* provides an advantage.

RESULTS

Zetaproteobacteria produce Fe(III) oxyhydroxide tubular sheaths in Fe mats at Fåvne

The porous black smoker chimneys at Fåvne show focused flow venting at 227°C of fluids containing abundant Fe(II) and H_2 (55), and support growth of extensive Fe mats covering tall black smoker chimney spires (Fig. 1a and b). The temperature within the Fe mats close to the venting orifice on chimney exteriors was measured at ~50°C (Fig. 1b). The chimney structures appear to lack defined central conduits (54), leading to copious venting of hydrothermal fluids (55) through permeable and porous chimney walls. Analysis of the microbial community composition based on metagenome-assembled genome (MAG) coverage (and supported by 16S sequence read abundance) revealed that Zetaproteobacteria comprised 7% of the observed community (Fe Mat, see Supplementary Material 1 Table S1 at https://doi.org/10.5281/zenodo.8297777).

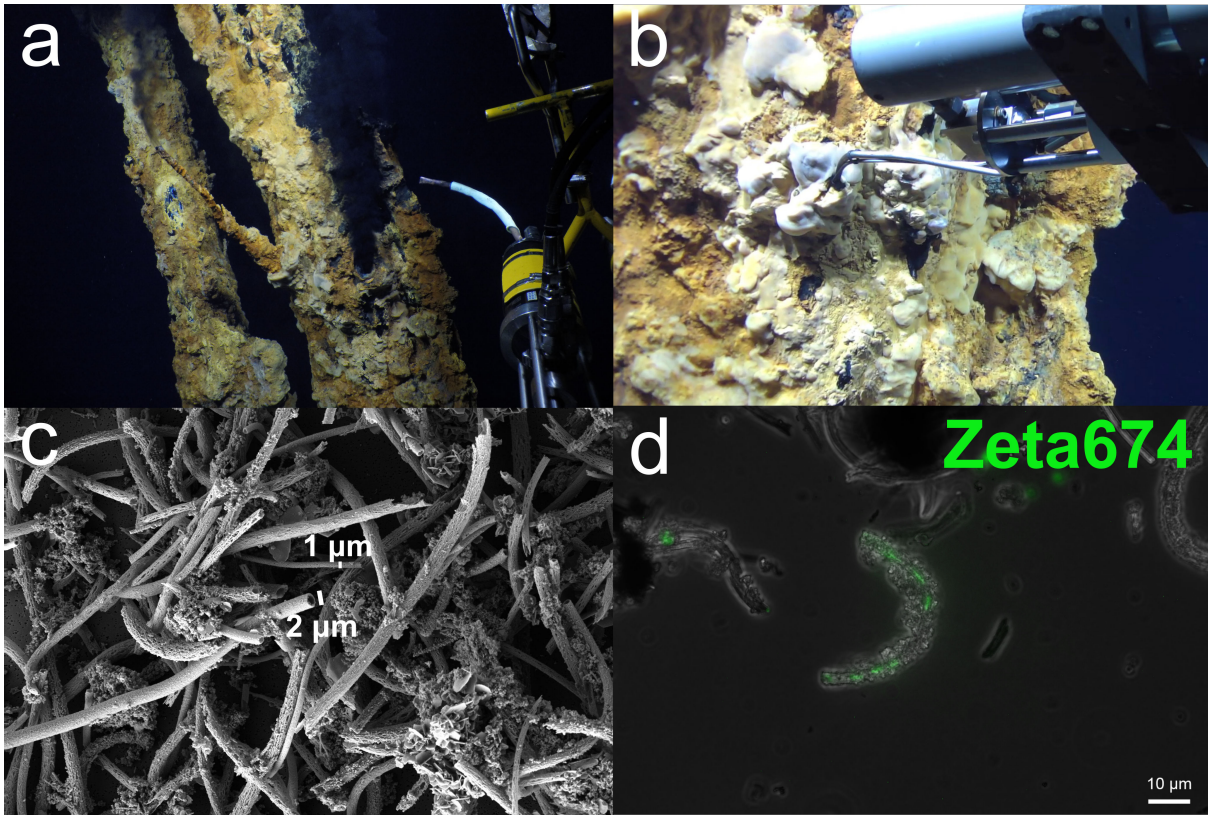

FIG 1 Fe mats at Fåvne are dominated by Fe(III) oxyhydroxide sheaths produced by Zetaproteobacteria. (a) Fe mats on black smoker chimneys at Fåvne vent field with hydraulic suction device (biosyringe) used for sampling on the right. (b) Measuring temperatures within Fe mats using an isobaric gas-tight sampler (55). (c) Fe mats dominated by Fe(III) oxyhydroxide sheaths of two different widths produced by Zetaproteobacteria, scanning electron microscopy. Two Fe(III) oxyhydroxide sheath morphotypes, either 2 µm or 1 µm wide. (d) Zetaproteobacteria cells inside Fe(III) oxyhydroxide sheaths (stained with Zeta674 fluorescence *in situ* hybridization probe). Overlay of phase-contrast and florescence images.

Other lineages frequently observed at vents (58–62) were more abundant in the Fe mat sample than Zetaproteobacteria, including members of Gammaproteobacteria and Campylobacterota (previously known as Epsilonproteobacteria [63]) of mainly genus *Sulfurovum*, which comprise 31% and 30% of the community, respectively (see Fig. S1 at https://doi.org/10.5281/zenodo.8297777). A single Alphaproteobacteria *Robiginitomaculum* MAG comprised ~2% of all MAGs recovered from the mat sample. Three high-quality (CheckV) viral genomes (vMAGs) identified in the Fe mat are predicted to have abundant Fe mat bacteria *Sulfurimonas* (Campylobacterota) and Gammaproteobacteria as potential hosts (see Table S1 at https://doi.org/10.5281/zenodo.8297777).

Scanning electron microscopy (SEM) revealed that tubular Fe(III) oxyhydroxide sheaths dominate the black smoker Fe mats (Fig. 1c, see Fig. S2 and S3 at https://doi.org/10.5281/zenodo.8297777). Fe(III) oxyhydroxide sheaths were the only morphotype observed, the majority of which are about 2 µm wide, with thinner 1 µm sheaths also present, albeit less frequently. The Zeta674 fluorescence *in situ* hybridization (FISH) probe detected Zetaproteobacteria cells inside the sheaths (Fig. 1d), identifying tubular sheath-forming Zetaproteobacteria as major Fe-oxidizers in the Fe mat.

Phylogeny of Fe-oxidizing Zetaproteobacteria at Fåvne

Out of 111 MAGs reconstructed from the Fe mat, dereplicated at 98% ANI, with average completeness of 91.1% and average contamination of 1.9% (see Table S2 at https://doi.org/10.5281/zenodo.8297777), 69 MAGs were of high quality (>90% completeness, <5% contamination), and 42 MAGs were of medium quality (>50% completeness, <10% contamination) (64). Five of all the MAGs from the Fe mat were classified as the Zetaproteobacteria genus *Ghiorsea* (Genome Taxonomy Database [GTDB] and 16S sequences). All but one of the *Ghiorsea* MAGs are new species-representative genomes based on publicly available genomes of Zetaproteobacteria and a 95% average nucleotide identity (ANI) cutoff (65, 66). Phylogenomic and average amino acid identity (AAI) analyses among *Ghiorsea* identified two distinct clusters previously not described for the genus (designated Clusters A and B, Fig. 2, see Fig. S4 at https://doi.org/10.5281/zenodo.8297777). The two Fåvne MAGs in Cluster A were affiliated with the symbiont *Ghiorsea* from the vent shrimp *Rimicaris* (67), *Ghiorsea* from Mid-Cayman Rise and North Pond (68), whereas the three other Fåvne MAGs in Cluster B were affiliated with the cultivated *G. bivora* (53) and *Ghiorsea* from Urashima (31). The two dominating *Ghiorsea* Fåvne MAGs, Faavne_M6_B18 and AMOR20_M1306, are members of each of these clusters and were present at 5% and 2%, respectively. Based on ANI estimates, the closest publicly available genome to the highest-quality *Ghiorsea* MAG from Fåvne (98.5% completeness, 2.6% contamination) is a *Ghiorsea* MAG (64.8% complete) from a cold oxic subseafloor aquifer (68) with an ANI value of 81.3% (see Fig. S5 at https://doi.org/10.5281/zenodo.8297777). The same Fåvne MAG has an ANI value of 77.7% to *Ghiorsea bivora* (53), an isolated Zetaproteobacteria ZetaOTU9 representative, while the 16S sequence has 96.8% identity to the isolate sequence.

To compare the taxonomy of Zetaproteobacteria in Fe mats with those present at other locations at Fåvne, we recovered MAGs from other Fåvne sampling sites (see Supplementary Material 1 Table S1 at https://doi.org/10.5281/zenodo.8297777). While black smoker Fe mats Zetaproteobacteria were all assigned to the genus *Ghiorsea*, low-temperature diffuse venting at Fåvne supported a higher number of other Zetaproteobacteria taxa (see Table S3 at https://doi.org/10.5281/zenodo.8297777). A total of 28 unique species-representative genomes of Zetaproteobacteria were recovered at Fåvne (based on 95% ANI cutoff and publicly available MAGs) consisting of high- and medium-quality MAGs (average completeness 81.7%, contamination 2.1% based on CheckM2; see Table S4 at https://doi.org/10.5281/zenodo.8297777). These Fåvne MAGs were associated with two families defined by GTDB and seven defined genera, with three MAGs remaining unclassified to genus level and most of taxa lacking cultured representatives (see Fig. S6 at https://doi.org/10.5281/zenodo.8297777).

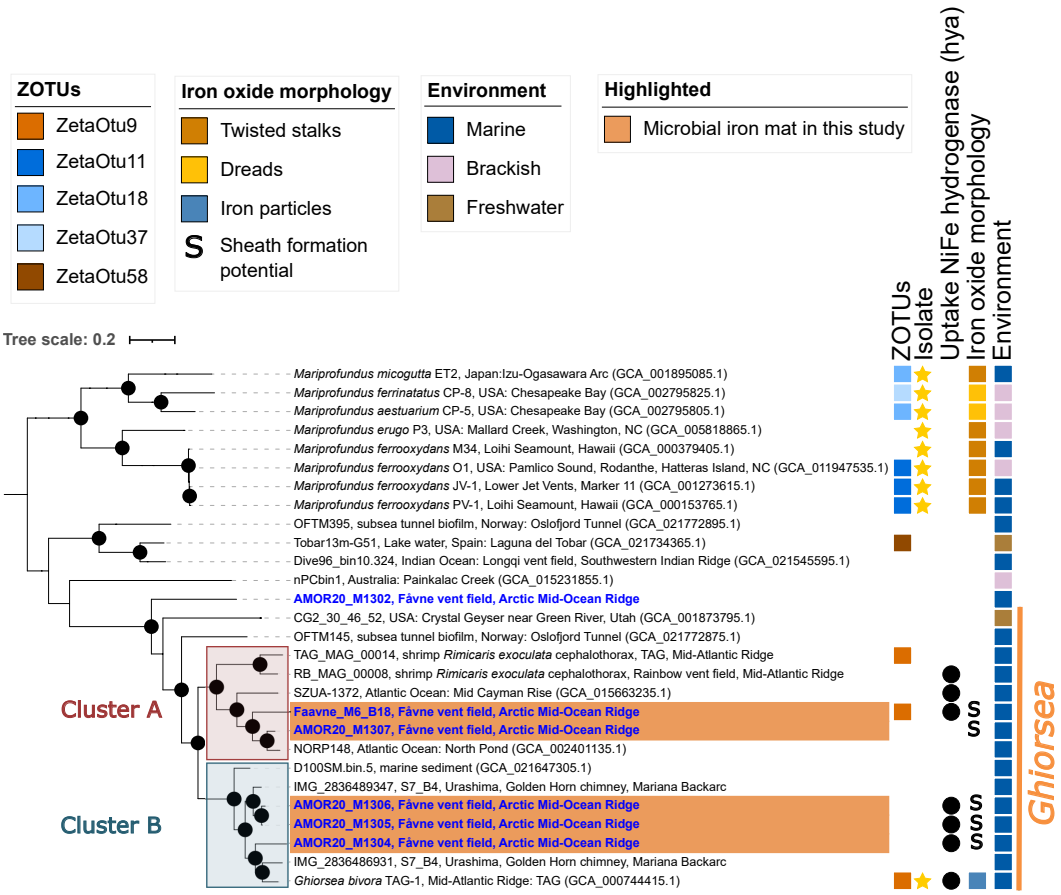

FIG 2 Phylogeny of Zetaproteobacteria in black smoker Fe mats at Fåvne. The tree is based on a concatenated alignment of a manually curated set of 12 single-copy gene markers (see Table S5 at https://doi.org/10.5281/zenodo.8297777) using MAGs from this study and references. Blue genomes have been reconstructed from the Fåvne vent field. Genomes highlighted in orange are present in Fe mat associated to a focused flow black smoker (*Ghiorsea*, ZetaOTU9). MAGs above 0.5 coverage were selected. Black node circles mark branches with support values higher than 75% with standard bootstrapping and 1,000 iterations. The maximum likelihood tree with substitution model Qpfam + F + I + I + R7. The *Ghiorsea* genus is based on GTDB taxonomy r214 and AAI values within the proposed 65% AAI cutoff for genus (69).

Ghiorsea in Fåvne Fe mats can oxidize H_2 in addition to Fe(II)

In alignment with the presence of H_2 and Fe(II) in endmember fluids at Fåvne (55), genes encoding all subunits of a transmembrane H_2-uptake Ni,Fe hydrogenase (Group 1d) and Cyc2 for Fe(II) oxidation were identified in Fåvne *Ghiorsea* genomes belonging to both Cluster A and Cluster B (Fig. 2 and 4). In addition, codon usage bias analysis predicts high expression of Fe(II) oxidation and H_2 oxidation genes of the *Ghiorsea* MAGs from Fåvne (see Table S5 at https://doi.org/10.5281/zenodo.8297777). A broader functional screening revealed that H_2-based metabolism with a Group 1d hydrogenase is common to other dominant MAGs within the Fe mat belonging to the Gammaproteobacteria, Ignavibacteria, Calditrichia, KSB1, and Aquificae (see Fig. S7; Table S6 at https://doi.org/10.5281/zenodo.8297777). *Ghiorsea* and some Gammaproteobacteria in the Fe mat also encode genes of an Ni,Fe H_2-sensing hydrogenase histidine kinase-linked Group 2b (*hup*) located in the cytosol responsible for activating hydrogenase expression (see Fig. S8 at https://doi.org/10.5281/zenodo.8297777) (70). In contrast, hydrogenases were not detected in Zetaproteobacteria MAGs not belonging to genus *Ghiorsea* from other locations at Fåvne.

A phylogenetic tree constructed using the large subunit of the transmembrane Ni,Fe hydrogenase (Fig. 3, see Fig. S7 at https://doi.org/10.5281/zenodo.8297777) to assess the evolutionary relationships of encoded hydrogenases reveals the close relationship

of Fåvne *Ghiorsea* hydrogenases with hydrogenases of other *Ghiorsea* (53, 67) and Gammaproteobacteria. Interestingly, the closest non-Zetaproteobacteria homolog was identified as a hydrogenase from a Gammaproteobacteria MAG (encoding genes for sulfur oxidation) from the same Fe mat.

The *cyc2* gene has previously been identified as one of the key genes in Fe(II) oxidation, with three distinct phylogenetic clusters of functionally verified and

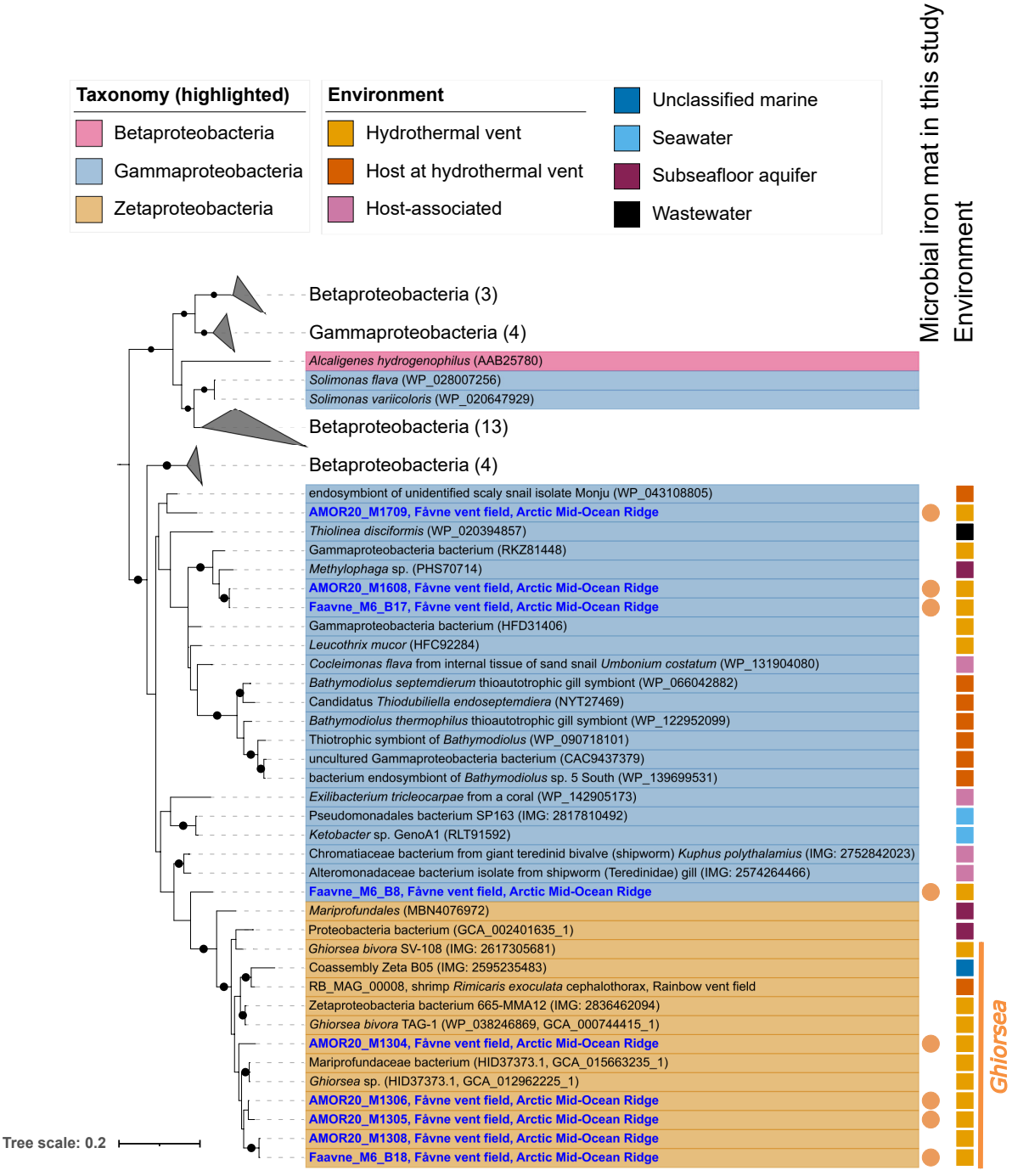

FIG 3 Phylogeny of the large subunit of uptake Ni,Fe hydrogenase (hya; 1d). Phylogenetic tree of the large subunit of uptake Ni,Fe hydrogenase (hya; 1d) present in MAGs in the black smoker Fe mat and in all publicly available Zetaproteobacteria genomes, with closest relative reference using BLAST. Blue MAGs have been reconstructed from the Fåvne vent field. Black node circles mark branches with support values higher than 75% with standard bootstrapping and 1,000 iterations. Maximum likelihood tree with substitution model LG + I + I + R7.

biochemically characterized representative Fe oxidases (51, 71, 72). Identified Cluster 3 and Cluster 1 *cyc2* genes of *Ghiorsea* in the Fe mat at Fåvne showed highest similarity to *cyc2* in other *Ghiorsea* MAGs from hydrothermal vents. Cyc2 genes were also identified in MAGs belonging to Gammaproteobacteria, Alphaproteobacteria, Aquificae, Planctomycetes, and Calditrichia (Fig. 4, see Table S7 at https://doi.org/10.5281/zenodo.8297777).

Manganese and iron are well known to co-vary in high-temperature black smoker fluids (73). Gene annotations revealed the presence of several genes in Gammaproteobacteria putatively involved in manganese oxidation, such as *mcoA, mopA,* and *moxA* (74–78). Furthermore, preliminary proteomics analysis of abundant proteins in black smoker Fe mats shows expressed McoA (see Table S8, Supplementary Material 2 Text1 at https://doi.org/10.5281/zenodo.8297777).

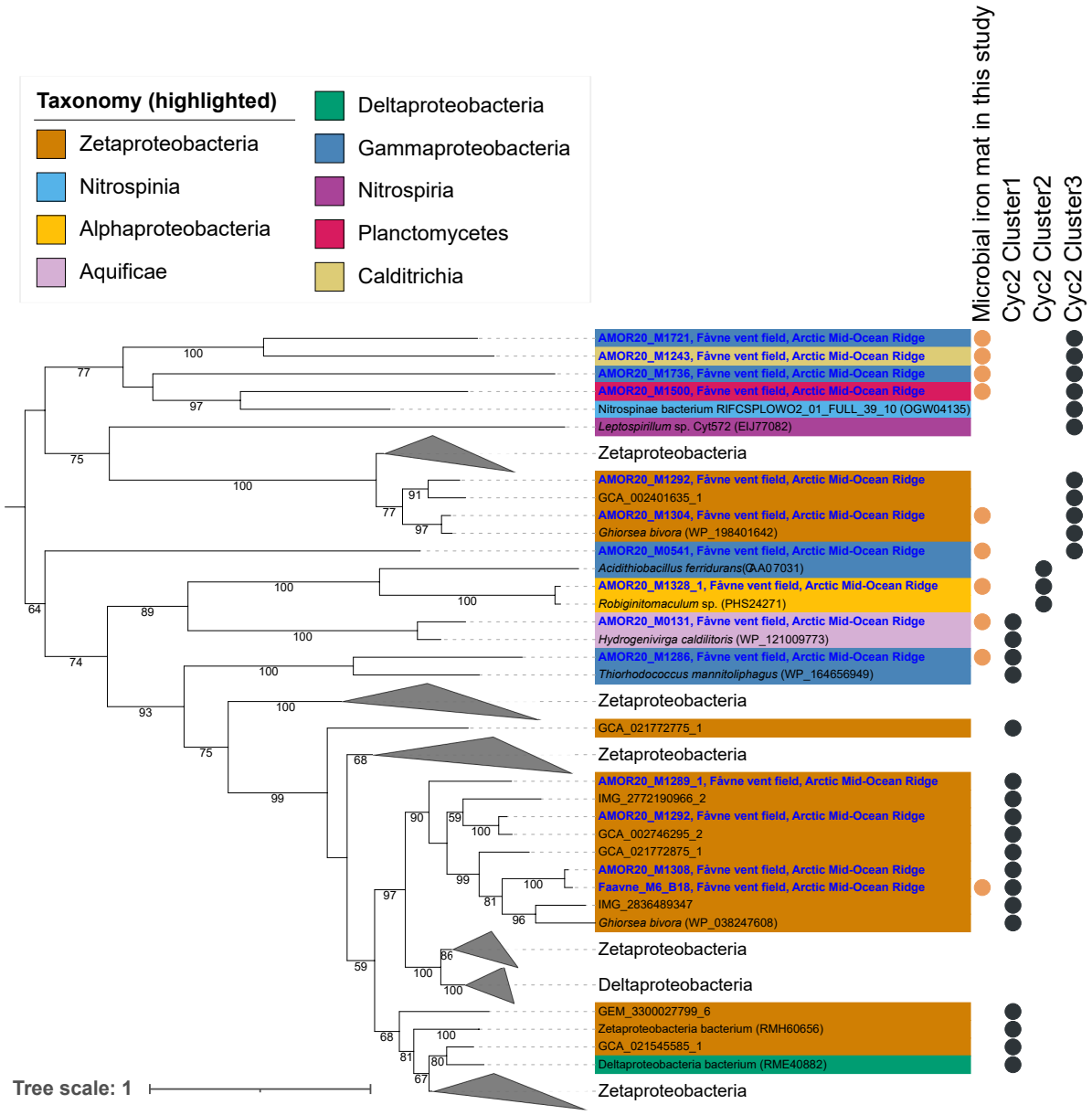

FIG 4 Phylogeny of outer membrane cytochrome Cyc2. Phylogenetic tree of Fe oxidation cytochrome Cyc2 present in MAGs in the black smoker Fe mat including amino acid sequences from all publicly available Zetaproteobacteria genomes with closest relative references using BLAST. Blue labels are sequences from MAGs reconstructed from the Fåvne vent field in the current study. Support values for branches are calculated with standard bootstrapping and 1,000 iterations. The maximum likelihood tree was constructed using the substitution model Qpfam + F + I + I + R5.

Metabolism of the microbial community in Fe mats

Analysis of the genomic content of the 25 most abundant MAGs (see Table S2 at https://doi.org/10.5281/zenodo.8297777), contributing to 87% of the binned coverages, identified genes for the oxidation of sulfur compounds, H_2, CH_4, and NH_4^+ (Fig. 5, see Fig. S9 at https://doi.org/10.5281/zenodo.8297777). Terminal oxidases found in *Ghiorsea* MAGs were cbb3-type cytochrome c oxidases, indicating an adaptation to low oxygen concentrations (79). Other MAGs contained both cbb3-, aa3-type cytochrome c oxidases, and cytochrome bd-I ubiquinol oxidases. Dissimilatory nitrate and nitrite reductase genes were identified in *Ghiorsea* MAGs, indicating a possibility of an auxiliary anaerobic metabolism (19, 80). Arsenate reductase was also detected.

Enzymes involved in carbon fixation were identified (see Fig. S10 at https://doi.org/10.5281/zenodo.8297777) for expected CO_2 fixation pathways in representative lineages (40, 63, 81, 82); however, key genes for the serine variant of the reductive glycine pathway were observed in a Campylobacterota MAG (83). Form I RubisCO genes were identified in the *Ghiorsea* MAG Faaavne_M6_B18, and in a Gammaproteobacteria and Alphaproteobacteria MAG, using LithoGenie within MagicLamp (84). In one Alphaproteobacteria MAG, gene for Form II RubisCO was also identified.

Given that Fe(III) oxyhydroxides adsorb heavy metals (5), an analysis of heavy metal resistance genes within the full metagenomic assembly of the Fe mat was performed. Heavy-metal resistance genes were identified for copper, cobalt, sodium acetate, chromium, tellurium, selenium, and silver (see Table S9 at https://doi.org/10.5281/zenodo.8297777).

DISCUSSION

Fe-oxidizing Zetaproteobacteria are globally distributed, yet our knowledge on the importance of hydrogen for their distribution is still limited. Here, we phylogenetically and functionally characterized Fe(II)- and H_2-oxidizing Zetaproteobacteria from the Fåvne vent field belonging to *Ghiorsea* genus, adding four novel species-representative genomes predicted to use H_2. We reconstructed 28 novel species-representative genomes of diverse Zetaproteobacteria taxa, extending the known Zetaproteobacteria

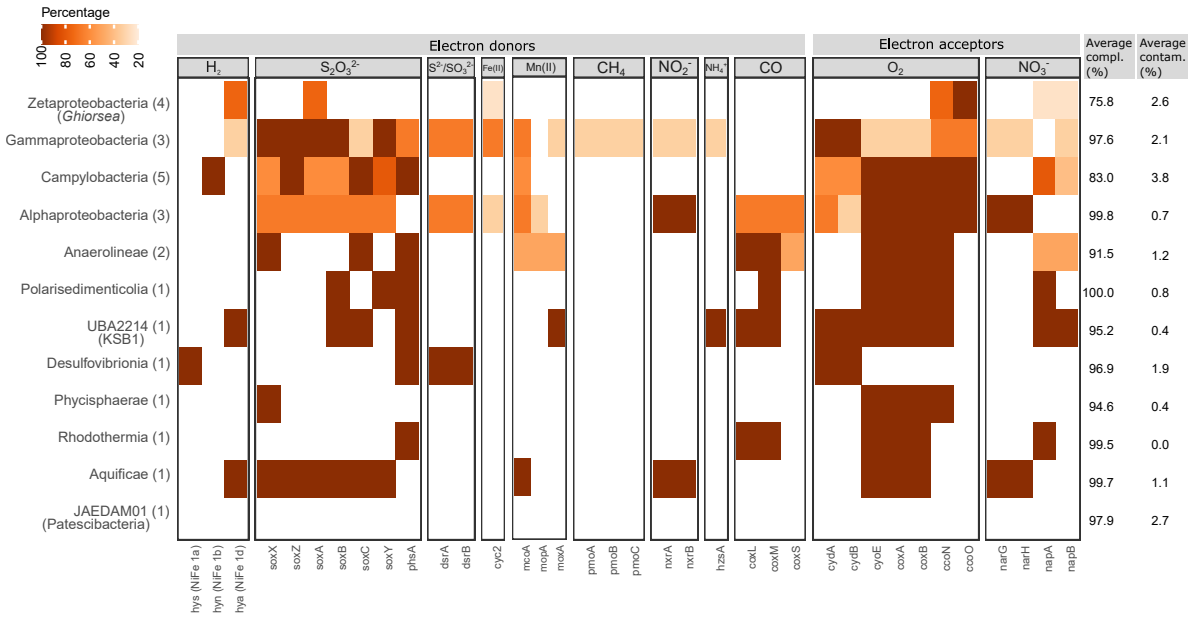

FIG 5 Functional characterization of the top 25 abundant MAGs in the black smoker Fe mat. Distribution of genes involved in the utilization of a range of electron donors and electron acceptors. The number of genomes in each taxonomic class cluster is indicated in parenthesis, and the color gradient refers to the percentage of genomes per class that encode the genes. Average completeness and contamination values for each taxonomic class cluster are based on CheckM2 predictions. Top 25 most abundant MAGs account for 87% of MAG coverages.

diversity. Based on Zetaproteobacteria distribution at Fåvne and encoded uptake hydrogenases, we demonstrate that H_2 availability indeed plays a role in the niche diversity of Zetaproteobacteria. Multiple species of *Ghiorsea* share the H_2 oxidation capacity in Fe mats at Fåvne, possibly sharing one niche.

Until recently, the identity of sheath-forming Zetaproteobacteria has remained elusive. We show that at least two populations of *Ghiorsea* (ZetaOTU9) most likely produce Fe(III) oxyhydroxide sheaths and form dense Fe mats.

Hydrogen as a driver of Zetaproteobacteria diversification

Most Zetaproteobacteria genera are metabolic specialists only able to obtain energy from the oxidation of Fe(II). The only known cultivated exception is *G. bivora,* capable of using H_2 simultaneously with Fe(II), or as sole electron donor (53). It has been suggested that members of *Ghiorsea* (ZetaOTU9) not only occupy environments rich in Fe(II) but also combined with predicted presence of H_2, such as at hydrothermal vents (53), in corrosion of steel (8, 85), and mineral weathering (40, 85, 86). The presence of hydrogen in these *Ghiorsea* environments has mainly been based on hypotheses until the current study. Remarkably, in the Fe mat close to the venting orifice at Fåvne and in contact with fluids containing abundant H_2, the reconstructed Zetaproteobacteria MAGs are represented by only *Ghiorsea* within ZetaOTU9.

In contrast, a higher diversity of Zetaproteobacteria is present in low-temperature diffuse-venting areas at around ~10°C (see Table S3; Fig. S11 and S12 at https://doi.org/10.5281/zenodo.8297777). All these genomes, except for *Ghiorsea*, lack uptake hydrogenases (see Fig. S6 at https://doi.org/10.5281/zenodo.8297777). Low-temperature diffuse-venting areas may reflect a low availability of H_2 relative to Fe(II), lost by abiotic or other subsurface mixing processes and low-temperature fluid formation (87). *Ghiorsea*, with its hydrogen uptake capability, emerges as the sole specialist in the presence of H_2. Members within *Ghiorsea* are also observed in likely H_2-poor diffuse-flow environments. Here, the diversity of Zetaproteobacteria is higher, also reflected by a diversity of Fe(III) oxyhydroxide structures (see Fig. S13 and S14 at https://doi.org/10.5281/zenodo.8297777). Hence, this diversity indicates an absence of a monopolizing niche player in H_2-poor diffuse flow, in contrast to *Ghiorsea* in the black smoker Fe mat where H_2 is available. This pattern of distribution supports the hypothesis that H_2 acts as a niche-determining factor for *Ghiorsea* at Fe(II)-rich hydrothermal vents (40). The ability of *Ghiorsea* to utilize H_2 affords it a competitive advantage as H_2 is a thermodynamically more favorable energy source than Fe(II), supporting faster cell growth (53). The competitive advantage of growing on H_2 is likely linked to evading the need for reverse electron flow to replenish the reducing agent NADH needed for CO_2 fixation (Fig. 6).

Hydrogenases restricted to *Ghiorsea* ZetaOTU9 at Fåvne show that potential for growth on H_2 is a trait limited to ZetaOTU9. However, through the analysis of publicly available genomes of Zetaproteobacteria, transmembrane uptake hydrogenases were detected in Zetaproteobacteria outside of *Ghiorsea*, beyond hydrothermal vents (see Fig. S6 and S7 at https://doi.org/10.5281/zenodo.8297777). Even so, all *Ghiorsea* do not necessarily share the ability to oxidize H_2. Outside of *Ghiorsea* Clusters A and B, two species representatives of *Ghiorsea* from freshwater and a subsea tunnel do not appear to possess hydrogenases (Fig. 2). Thus, far evidence suggests that presence of hydrogenases within *Ghiorsea* may be unique to hydrothermal vents.

Other H_2 oxidizers besides *Ghiorsea* are also present in the black smoker Fe mat which possess different hydrogenases (Fig. 5). Ni,Fe hydrogenases found in *Ghiorsea* MAGs were most closely related to hydrogenase subunits from other *Ghiorsea* and a Gammaproteobacteria MAG within the same Fe mat (Fig. 3) and symbiont chemolithotrophic sulfur-oxidizing microorganisms in hydrothermal vent fauna. These observations further strengthen the possibility of horizontal gene transfer of H_2 oxidation genes between Zetaproteobacteria and lithotrophic sulfur-oxidizing Gammaproteobacteria (53). We hypothesize this may have happened at hydrothermal vents.

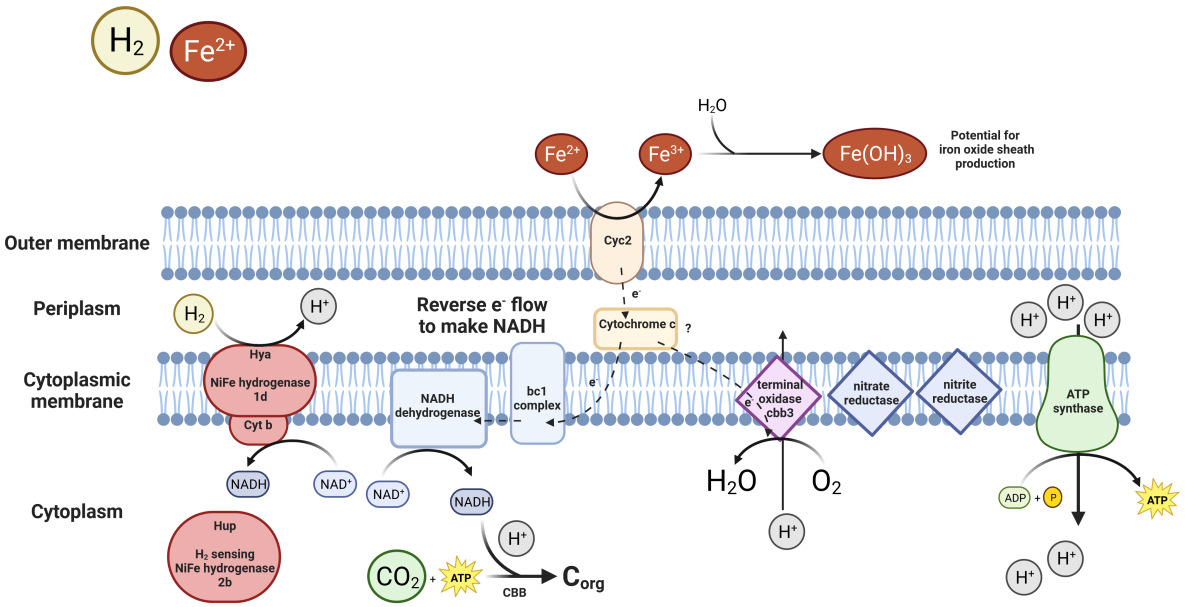

FIG 6 Membrane complexes in *Ghiorsea*. Electrons coming from the oxidation of Fe^{2+} are passed all the way to the high oxygen affinity terminal oxidase, leading to the generation of a proton motive force. Reverse electron transport is necessary to regenerate NADH needed for CO_2 fixation. NADH could also get replenished with the help of Ni,Fe uptake hydrogenase instead of the energy-intensive reverse electron transport. Hydrogenase can also donate electrons to the electron transport chain. ATP is generated by ATP synthase. A schematic representation of the metabolic potential of *Ghiorsea*, based on *Ghiorsea* MAGs from Fåvne and previous studies (40, 53). Created with BioRender.com.

Fe mats at Fåvne cover black smokers at temperatures of up to 50°C (the maximum measured inside of a single Fe mat), which is at the high end of the temperature spectrum where Fe mats and ZetaOTU9 have been observed (40, 53). The role of temperature in distribution patterns of Zetaproteobacteria cannot be ignored; however, minor differences in predicted optimum growth temperatures (see Fig. S6 at https://doi.org/10.5281/zenodo.8297777) indicate fluid composition plays a larger role on the *Ghiorsea* (ZetaOTU9) niche differentiation than temperature. It is worth noting that the Fe mat studied is a bulk sample, where different microenvironments likely exist with varying degrees of exposure to the high-temperature-reducing venting fluids. Obtaining small-scale samples and corresponding *in situ* measurements to capture this variability in such environments remains a challenge.

Several *Ghiorsea* populations at Fåvne share the same metabolic niche

Within the Fe mats at Fåvne, four novel uncultured species or populations represented by MAGs of *Ghiorsea* (ZetaOTU9) co-exist, belonging to two distinct phylogenetic clusters (Cluster A and Cluster B; Fig. 2). Co-existence of multiple *Ghiorsea* populations has also been observed in *Rimicaris* vent shrimp, where the difference in the presence of hydrogenase in *Ghiorsea* MAGs has been proposed to contribute to niche partitioning, avoiding potential competition (67). In contrast, at Fåvne, all species-representative *Ghiorsea* genomes seem to possess genes for common metabolic functions, including presence of uptake hydrogenases, suggesting that multiple *Ghiorsea* species occupy the same ecological niche at Fåvne. It remains unknown what kind of interactions arise from co-occupying the niche in Fe mats. Possible competitive relationships among closely related populations of Zetaproteobacteria could be responsible for differential distribution across physical space ultimately leading to divergence within the ZetaOTU, as hypothesized for cosmopolitan ZetaOTU2 (88). In this context, the use of genome-

resolved metagenomics offers valuable information about distinct subpopulations belonging to the same ZetaOTU and their genomic makeup.

Production of Fe(III) oxyhydroxide sheaths by members of the Fe- and H_2-oxidizing genus *Ghiorsea* (Zetaproteobacteria)

In contrast to stalk-forming Zetaproteobacteria (44), the identity of sheath-forming Zetaproteobacteria has not been established through either cultivation or identification of the environmental and genetic drivers for sheath formation. Fe(III) oxyhydroxide sheaths in marine environments were shown to be associated with Zetaproteobacteria (18), and previous research has suggested ZetaOTU6, ZetaOTU9, and ZetaOTU15 as candidates for sheath-forming Zetaproteobacteria (22, 24, 85), with ZetaOTU6 sequences identified from an enrichment of sheath-forming Zetaproteobacteria (85). Specific ZetaOTU could not definitively be assigned to sheath morphology; however, ZetaOTU2, ZetaOTU6, and ZetaOTU14 were present in sheath-rich Fe mats (18). *Ghiorsea* within ZetaOTU9 accounting for 100% of all Zetaproteobacteria present in the Fe mat and the abundant homogenous Fe(III) oxyhydroxide tubular sheaths containing Zetaproteobacteria cells (Fig. 1d, see Fig. S11 and S14 at https://doi.org/10.5281/zenodo.8297777) strongly suggest that, at Fåvne *Ghiorsea,* ZetaOTU9 is uniquely forming these structures. The presence of two-size morphotypes of Fe(III) oxyhydroxide sheaths suggests that more than one *Ghiorsea* population is producing Fe(III) oxyhydroxide sheaths. The comparison of MAG relative abundances with abundance of the two sheath variants (Fig. 1c) indicates the large 2 µm sheaths are produced by the Faavne_M6_B18 (Cluster A) *Ghiorsea* population, while the 1-µm-wide sheaths are produced by the AMOR20_M1306 (Cluster B) *Ghiorsea* population. Variable width Fe(III) oxyhydroxide sheaths hypothesized to be created by two different unidentified Zetaproteobacteria have previously been observed in Fe mats at Beebe's vents (34). Despite these concurring observations, the possibility remains that variation in sheath width is instead a consequence of a later, secondary colonization of the same species under different conditions, resulting in variations in cell size. Due to sheathed cells themselves being relatively rare and usually observed only at the tip of the sheaths while producing these structures moving forward (18), we cannot completely exclude the possibility that sheaths could be produced by a different rare ZetaOTU that was not detected in sequencing. Nonetheless, only through cultivation and targeted FISH staining, the formation of Fe(III) oxyhydroxide sheaths by *Ghiorsea* can be confirmed.

Similar to stalk formation, the genetic features for dread-forming Zetaproteobacteria are associated with the presence of distant homologs of stalk-forming Zetaproteobacteria *sfz* genes (44, 45). However, no homologs of the *sfz* genes were identified in *Ghiorsea* MAGs from Fåvne (Sfz1-6 genes; see Fig. S6 at https://doi.org/10.5281/zenodo.8297777) or the full metagenome assembly even at low sequence identity, suggesting a different genetic mechanism for sheath formation.

Whether sheaths are uniquely formed by *Ghiorsea* ZetaOTU9 globally remains an open question. Previous microscopy studies of *Ghiorsea* did not reveal any sheath formation (53, 67), with the cultured representative strains of *Ghiorsea* instead producing amorphous Fe(III) oxyhydroxide particulates during growth on $FeCl_2$ (53). This aligns with the observation that closely related species vary in their capacity to produce distinct Fe(III) oxyhydroxide structures (20). Sheath-dominated Fe mat communities have been observed at several locations (18, 20, 23, 24, 32, 34). Given that ZetaOTU9 has been described as having a cosmopolitan distribution (22, 35, 89), member species could be producing Fe(III) oxyhydroxide sheaths in numerous environments worldwide. This emphasizes the importance of microscopy in microbial ecology as not everything can be easily observed through genetic analyses. As preserved biogenic Fe(III) oxyhydroxide structures can help us understand the environmental conditions of early Earth through studying ancient iron oxide deposits (90–93) and can also be potentially used as biosignatures (20, 94), knowledge of a sheath-forming Zetaproteobacteria capable of oxidizing both Fe(II) and H_2 might prove valuable for the interpretation.

Ghiorsea (ZetaOTU9) is the architect of Fe mats with abundant H_2

Although sheath-forming *Ghiorsea* is not the most abundant community member (7% relative abundance), it can be considered the main community engineer with respect to the amount of produced material (Fig. 7), in agreement with Zetaproteobacteria previously characterized as ecosystem engineers and primary colonizers in Fe mats (20, 95). The generation of the architectural character of the Fe mat is subsequently followed by recruitment of other community members (42). At Fåvne, the dense Fe mats close to the venting orifice show a high abundance of Campylobacterota (formerly Epsilonproteobacteria), Gammaproteobacteria, and Alphaproteobacteria; taxa commonly seen in Fe mats (27). Diversity of primary producers in Fe mats at Fåvne appears high in comparison with other hydrothermal vent mats dominated by sulfur oxidizers (59–61). This is in-line with previous findings that FeOB support higher diversity (20, 27). Differences in relative abundances of common lineages in microbial mats have been

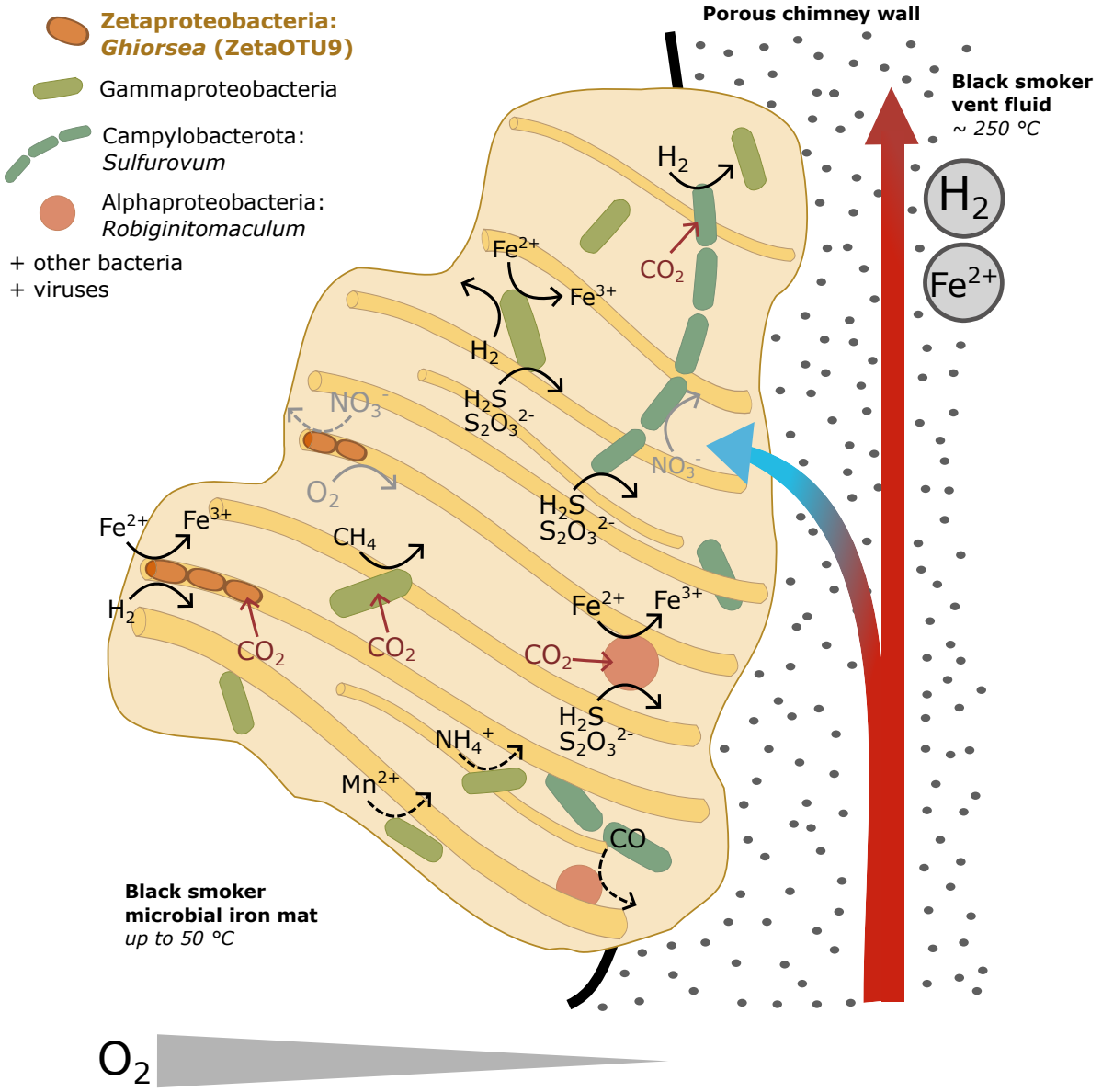

FIG 7 Conceptual model of Fe mats on black smoker chimneys at Fåvne vent field. Fe mats are found on black smoker chimneys with focused flow high-temperature venting of fluids containing iron and hydrogen. The temperature in the Fe mat close to the chimney exterior was ~50°C. The model is based on metabolic reconstruction of MAGs of the most abundant microbial groups.

observed at sites with differing chemistry in previous studies (27, 88, 96), emphasizing the influence of vent fluids on microbial mat communities.

The mixing of oxygen-rich seawater and reduced vent fluids in the porous chimney structures at Fåvne gives rise to steep chemical gradients which are reflected in the available electron donors and acceptors utilized within the Fe mat (Fig. 5). A strong association of Fe and Mn has been shown for hydrothermal fluids elsewhere (73), and at Fåvne, genes likely involved in manganese oxidation or detoxification were detected in proteomics analysis (Fig. 5, see Table S8, Supplementary Material 2 Text 1 at https://doi.org/10.5281/zenodo.8297777). Consistent with the notion that Fe(III) oxyhydroxides adsorb heavy metals (5), the presence of various heavy metal resistance genes in the Fe mat (see Table S9 at https://doi.org/10.5281/zenodo.8297777) suggests adaptation to heavy metals.

Diversity of Fe oxidation based on Cyc2 genes at Fåvne

Potential for iron oxidation at Fåvne vent field is not limited to Zetaproteobacteria based on the presence of Cyc2 genes across several phyla. The identification of *cyc2* in abundant members of the Gammaproteobacteria and Alphaproteobacteria may indicate a broader taxonomic range for neutrophilic iron oxidation (Fig. 4 and 5), as seen in previous studies (31, 51, 52, 85, 97, 98), including in vent fauna endosymbionts (45, 50). Based on metabolic profiling, MAGs possessing *cyc2* seem able to use oxygen and nitrate (Fig. 5, see Fig. S15 at https://doi.org/10.5281/zenodo.8297777). The presence of nitrate and nitrite reductase genes in Zetaproteobacteria MAGs suggests a possibility of an advantageous metabolic plasticity in Zetaproteobacteria able to reduce nitrate and nitrite in the absence of oxygen. Such an anaerobic metabolism has not yet been observed in isolates under laboratory conditions (19, 80),z and Zetaproteobacteria terminal oxidases are predicted to be highly expressed (see Table S5 at https://doi.org/10.5281/zenodo.8297777). Similarly, in addition to the common microaerophilic Zetaproteobacteria, anaerobic iron oxidizers have been detected in deeper layers of Fe mats at Kama'ehuakanaloa (Lō'ihi) (21). It remains unknown whether the widespread occurrence of Cyc2 genes at Fåvne is involved in Fe oxidation to obtain energy for carbon fixation in several lineages or whether some of these microorganisms rather use the Fe oxidase in other processes such as detoxification (52, 99). It is, however, unlikely that Fe-oxidizing *Ghiorsea* at Fåvne are competing with other organisms for Fe resources, as there is an abundant supply of Fe(II) in the venting fluids (55).

Most Zetaproteobacteria encode for Form II RubisCO (41, 48, 100, 101), including *Ghiorsea* genomes (53, 67), suggesting a preference for environments with high CO_2 and low oxygen concentrations (102, 103). A few Zetaproteobacteria encode genes for both Form I RubisCO, adapted to higher O_2 concentrations, and Form II RubisCO (48, 104, 105), suggesting a certain environment flexibility. Notably, *Ghiorsea* MAG Faaavne_M6_B18 (98.5% complete) encoded genes for Form I RubisCO exclusively, possibly indicating a tolerance to higher oxygen concentrations than most other Zetaproteobacteria. This oxygen tolerance could be in-line with their hypothesized presence on the outer, more oxygenated side of the black smoker Fe mat.

Porous black smoker chimneys support growth of Fe mats with iron and hydrogen at Fåvne

Previous studies of Fe mats constructed by Zetaproteobacteria have generally focused on low-temperature diffuse-venting areas rather than high-temperature hydrothermal vents (21, 22, 35). Although Fe mats on black smoker chimneys have been observed (29), the communities and interactions of their members have not yet been characterized. Whereas Fe mats studied previously are associated with fluids depleted in H_2 (18, 24, 27, 31), vent fluids at Fåvne contain both H_2 and Fe(II) as abundant energy sources for Fe mats growing on black smoker chimney surfaces (55). Other hydrothermal vents with similar geochemistry to Fåvne, such as Rainbow at Mid-Atlantic Ridge and Beebe's vents (Piccard) at Mid-Cayman Rise where both H_2 and Fe(II) are present, have chimneys that

contain much higher-temperature mineralized conduits that are likely not as porous (106, 107), which may establish a much steeper chemical gradient through the chimney walls that is unable to sustain large exterior Fe mats. In contrast, the chimneys at Fåvne appear to be highly porous, visibly allowing vent fluid to advect outward and permeate through to the chimney surface. This is evident by the relatively high measured exterior temperatures (50°C) and visible shimmering, compared with the often much lower, near bottom water temperatures typically observed on more mineralized chimney exteriors (108). We propose this high fluid flux setting creates a suitable environment for microbial life to access higher abundances of electron donors at warmer temperatures, thereby forming dense Fe mats.

Conclusion

The presence of abundant (mmolar) Fe(II) and H_2 in the hydrothermal fluids at the Fåvne vent field offers a unique opportunity to investigate the interactions and adaptations of FeOB in response to the presence of elevated H_2, providing valuable insights into their physiology and ecological dynamics. Our study is a first look into the microbial communities of black smoker Fe mats and the first microbiological exploration of the newly discovered Fåvne hydrothermal vent field. The findings strongly suggest that Zetaproteobacteria of Fe- and H_2-oxidizing genus *Ghiorsea* at Fåvne produce Fe(III) oxyhydroxide sheaths and form dense Fe mats. With these Fe(III) oxyhydroxide structures, *Ghiorsea* provide the environment for other microorganisms, ultimately maintaining the carbon, nitrogen, sulfur, and iron cycling in the Fe mats. Exclusive presence of Fe(II)- and H_2-oxidizing *Ghiorsea* in the black smoker Fe mat exposed to abundant H_2 compared with occupation by diverse Zetaproteobacteria without hydrogenases at likely low H_2 environments at Fåvne supports the notion that H_2 availability plays a crucial role in driving the niche partitioning of Zetaproteobacteria.

MATERIALS AND METHODS

Sampling site

The Fåvne vent field is located at 72°45.4′ N, 3°49.9′ E on the Mohns Ridge section of the series of AMOR at 3,030 m below sea level (54–56) (see Fig. S16 at https://doi.org/10.5281/zenodo.8297777). Black smoker chimneys have a porous structure and are rich in iron oxide and oxyhydroxide minerals, with high cobalt concentration of hydrothermal deposits (54, 56). The black smoker hydrothermal fluids there are characterized by abundant iron and hydrogen (55).

Sample collection

Iron microbial mat samples were collected using an Ægir6000 remotely operating vehicle (ROV) on board the R/V G.O. SARS in June 2019, equipped with a biosyringe (a hydraulic sampling cylinder) connected to the ROV manipulator arm (Fig. 1a). Temperature (±1°C uncertainty) in the iron microbial mat was taken in real time using a temperature probe attached to the isobaric gas-tight fluid sampler snorkel inlet (109), which was used for vent fluid sample collection (55). Iron microbial mat was collected on the exterior of the North Tower vent (coordinates 72°45.4′ N, 3°50′ E), a 13-m-tall active black smoker chimney 3,025 m below sea level, 1–2 m below the orifice (Fig. 1, see Supplementary Material 4, Supplementary Material 1 Table S1 at https://doi.org/10.5281/zenodo.8297777). Additional samples of the iron microbial mat mixed with underlying chimney, chimney, and iron oxide deposits were collected (see Supplementary Material 1 Table S1 at https://doi.org/10.5281/zenodo.8297777). Samples retrieved were centrifuged at 6,000 rcf for 5 minutes, and the supernatant was removed. Iron microbial mat pellet for on-ship metagenome sequencing using Nanopore MinION was processed directly. Aliquots for other analyses were frozen in liquid nitrogen and stored at −80°C until processing. Samples for scanning electron microscopy were fixed in 2.5%

glutaraldehyde and stored at 4°C until further processing. Samples for fluorescence microscopy were fixed in 2% formaldehyde at 4°C overnight.

Scanning electron microscopy and elemental composition analysis

Fixed samples for SEM were filtered onto 0.2 µm polycarbonate filters with subsequent incubation in a series of increasing ethanol concentrations to remove water with and without critical point drying in CO_2. Filters were then mounted on Al stubs and sputter coated with Ir using a Gatan 682 Precision etching coating system. The sputter coater was set for intended coating thickness of 10 nm. SEM images for morphological observation were produced at 5 keV using a Zeiss SUPRA 55VP scanning electron microscope equipped with a Thermo Noran Six Energy Dispersive Spectrometer at ELMILAB (laboratory for analytical electron microscopy) at the Department of Earth Science (Faculty of Mathematics and Natural Sciences, University of Bergen). For analysis of elemental composition, energy-dispersive X-ray spectroscopy (EDS) was performed at an accelerating voltage of 15 keV and a working distance of 8 mm. Data were processed with Pathfinder X-ray Microanalysis Software v.1.2 (Thermo Fisher Scientific) with default settings. Spot scanning setting was used, and Ir peaks were removed due to the Ir signal from the coating. Qualitative elemental abundances of all abundant elements were measured, with the focus on C, N, O, P, S, Fe, Mn, Cu, Ca, Mg, Al, Si, and Zn. Table of elements for EDS analysis was used to inform us whether there were elements with similar energies that could be mixed up.

Fluorescence *in situ* hybridization

Samples were fixed in 2% formaldehyde at 4°C overnight, rinsed three times with phosphate-buffered saline (PBS), resuspended in 1:1 PBS:ethanol solution, and stored at −20°C following a protocol for preservation of material for FISH (110). Samples were spread on microscopy slides, air dried, and embedded in 0.5% low melting point agarose. For visualizing Zetaproteobacteria, the Zeta674 probe labeled with Atto488 fluorochrome was used (18). The Zeta674 probe specificity was analyzed, and the probe was successfully hybridized *in silico* using the SILVA Test-Probe tool, local BLAST, and the 16S sequence of the highest-quality *Ghiorsea* MAG recovered (Faavne_M6_B18). FISH was performed according to a previously published protocol (111). Slides were incubated at 46°C for 1 h with 20% formamide hybridization buffer in a hybridization chamber. The probe was added, followed by hybridization for 2 h at 46°C. Slides were then incubated in a washing solution (0.1 M NaCl, 20 mM Tris-HCl [pH 8.0], 5 mM EDTA, and 0.01% SDS] at 48°C for 15 minutes, washed twice with PBS, and air dried. Vectashield antifade solution was added. Slides were visualized with fluorescence microscopy using an overlay of phase-contrast and fluorescence images. Non-EUB338 was used as a negative control (112). SYBRGreen was used to visualize all cells.

Genome-resolved metagenomics

On-ship Nanopore MinION sequencing workflow

DNA extraction, sequencing, and preliminary analysis were performed on board the research vessel during the expedition. DNA was extracted from a 1-mL Fe Mat sample aliquot using FastDNA Spin Kit for soil (MP Biomedicals), according to the manufacturer's protocol. Metagenomic sequencing of total DNA was carried out using the rapid sequencing library (SQK-RAD004) and the Oxford Nanopore Technologies MinION 1Mk1B sequencer equipped with a FLO-MIN106 SpotON Flow cell v.R9. Sequencing and raw data acquisition were controlled with the MinKNOW software. Basecalling was performed with a local version of the guppy basecaller v.3.4.4 (https://community.nanoporetech.com). Filtering of raw reads on length and quality was performed twice using Nanofilt v.2.5.0 as part of the NanoPack (113) and Porechop v.0.2.4 (https://github.com/rrwick/Porechop) (sequencing and filtering statistics in Tables S10 and S11 at https://doi.org/10.5281/zenodo.8297777).

Illumina sequencing workflow

Whole-sample genomic DNA was extracted using Powersoil DNA Isolation Kit (QIAGEN) from frozen samples and sent to the Norwegian Sequencing Centre (University of Oslo, Norway) for shotgun metagenomic sequencing. A 150-bp paired-end sequencing was performed using an Illumina NovaSeq S4 flow cell. Raw reads were scanned for quality, duplication rate, and adapter contamination using FastQC v0.11.9 (https://github.com/s-andrews/FastQC), and concurrent visualization of the reports across samples was carried out in MultiQC (114). Strand-specific quality filtering methods recommended (115) were implemented through use of the "iu-filter-quality-minoche" script of the illumina-utils python package (116). Quality-filtered reads were subsequently cleaned of contaminating human DNA by mapping reads to the hg19 human genome with a mask applied to highly conserved genomic regions using the bbmap.sh script within the BBTools package (117) and human genome mask developed by Bushnell (available at https://drive.google.com/u/0/uc?id=0B3llHR93L14wd0pSSnFULUlhcUk).

Sequence reads were assembled by individual metagenomic sample with MEGAHIT v1.2.9 (118) using a minimum contig length of 1,000 bp. Reads from each sample were consecutively mapped to individual Illumina sample assemblies, effectively "co-mapping," using Bowtie2 v.2.4.2 (119) then subsequent indexing with Samtools v.1.11 (120). Binning and quality procedures were identical to those carried out as detailed for MinION sequencing with the exception of inclusion of MaxBin2 v 2.2.4 as an additional binning software used before implementation of DASTool. File manipulation, contig database creation, and profiles were accomplished with scripts from the Anvi'o v.7 platform (121).

Metagenome assembly strategy

The assembly of the Nanopore-filtered reads was performed using the wtdbg2 v.2.5 long-read assembler (options: -p 21 -AS 2 s 0.05 L 2500--edge-min 2 --rescue-low-cov-edges) (122). Sequential polishing of the initial assembly was conducted twice with Racon v.1.4.3 (123) and Medaka v.0.8.2 (https://github.com/nanoporetech/medaka). Reconstruction of MAGs was performed in a combination using CONCOCT (124), MetaBAT (125, 126), and DASTool (127).

Hybrid assembly of Nanopore and Illumina reads was also performed using metaSPAdes (128). This hybrid assembly had lower quality than wtdbg2 and MetaFlye only and Illumina-polished MetaFlye assemblies (see Table S12 at https://doi.org/10.5281/zenodo.8297777), with lower quality bins and fewer 16S sequences assigned to the genomes. Nanopore-only-based assembly generated only the most abundant *Ghiorsea* MAG, while the MetaFlye assembly polished with Illumina reads recovered two *Ghiorsea* MAGs, one of them the same species representative (>95% ANI) as the most abundant one in the Nanopore-only assembly and another one, less abundant. With this in mind, we decided to go forward with the MetaFlye long-read assembly polished with Illumina reads. Assembly read information and quality metrics are shown in Table S12 at https://doi.org/10.5281/zenodo.8297777. Several other assembly and binning strategies were attempted and compared using QUAST v.5.0.2 with MetaQUAST output (129).

Combining long reads and short reads

To obtain high-quality metagenome-assembled genomes with better sequencing depth, a MetaFlye long-read assembly, done with Flye v2.9 and filtered Nanopore reads (130), was polished using Illumina short reads using Pilon v1.23 (131). Illumina short reads were mapped to the assembly using bwa v.0.7.17 (132) and minimap2 for Nanopore long reads (133). A mapping file was then reformatted using samtools (120). Automatic MAG reconstruction was performed using metaWRAP v.1.3 (134), which implements the combinatorial use of MaxBin2 (135), CONCOCT (124), and MetaBat2 (126). MAGs were manually refined using the Anvi'o v.7 platform (121). Quality and completeness of individual MAGs were assessed on the presence of lineage-specific, conserved single-copy marker genes using CheckM v1.0.7 (136) and CheckM2 v1.0.2 (137).

MAGs generated using MetaFlye, Pilon, and metaWRAP and the ones generated using only Illumina reads were dereplicated at 98% ANI using dRep v3.2.2 (138). These included all MAGs with at least 50% completeness and maximum 10% redundancy and all MAGs that had at least 0.5 coverage in the iron microbial mat metagenome (Fe Mat sample; 108 MEGAHIT Illumina MAGs and 19 MetaFlye, Pilon, and metaWRAP MAGs). The dereplication resulted in 111 MAGs. Relative abundances were calculated using the abundance output of relative coverage within one sample (Anvi'o v.7), and this was normalized to 1.

Taxonomic classification

The reconstructed MAGs were taxonomically classified using the genome taxonomy database tool kit gtdbtk v.2.3.2 (139) using the database GTDB 214 release. In addition, ZetaHunter v1.0.11 was used for assigning taxonomy to the 16S sequence of the Zetaproteobacteria MAGs (39), classifying sequences into Zetaproteobacteria operational taxonomic units at 97% similarity. Based on ZetaHunter cutoffs, we excluded all ZetaOTU classifications below 75% entropy. An overall taxonomic classification of Illumina metagenomic reads was performed with PhyloFLASH v.3.4 (140) based on 16S sequences using SILVA release 138 taxonomy as reference.

Genome database of Zetaproteobacteria

Zetaproteobacteria MAGs were reconstructed from samples of iron microbial mats, a chimney, and iron deposit at Fåvne (see Supplementary Material 1 Table S1 at https://doi.org/10.5281/zenodo.8297777). The choice was made to concentrate efforts on the black smoker Fe Mat after identifying the presence of only the genus *Ghiorsea* and iron oxide sheaths since Fe Mat was the most precise sample of the iron microbial mat. All publicly available Zetaproteobacteria genomes (74) (taxid 580370) and corresponding metadata at NCBI GenBank were downloaded using ncbi-genome-download v.0.3.0 (https://github.com/kblin/ncbi-genome-download/) on the 19 October 2021. In addition, publicly available genomes of Zetaproteobacteria were downloaded from Genomes from Earth's Microbiome (141), Joint Genome Institute Integrated Microbial Genomes (JGI IMG), and from public repositories stated in selected studies (21, 31, 67, 142). Additional genomes of Campylobacterota, Gammaproteobacteria, and Alphaproteobacteria closely related to the Fåvne MAGs were downloaded from NCBI as references. A threshold cutoff of high- and medium-quality genomes (min. 50% completeness, max. 10% redundancy) was used before further analysis. Phylogenomic analyses included 148 Zetaprotobacteria genomes in addition to the MAGs from this study. All selected genomes are presented in Table S4 at https://doi.org/10.5281/zenodo.8297777.

The combination of average nucleotide identity, average amino acid identity, and alignment fraction (AF) provides an objective measure of genetic relatedness between Zetaproteobacterial genomes. The proposed species cutoff at ~95% ANI (65, 66), ~95%–96% AAI (143), and 60% AF (144) was used, with the genus boundary at 65% AAI (69). ANI analysis based on the BLAST algorithm (ANIb) was performed using the anvi-compute-genome-similarity program within Anvio v.7.0 (121); --program pyANI --method ANIb (https://github.com/widdowquinn/pyani). AAI analysis was performed using ezAAI (145). AF was calculated using FastANI within Anvio. The graphical heatmap and dendrogram of percentage identities were plotted using gplots package in R.

Optimal growth temperatures were predicted for Zetaproteobacteria MAGs (see Fig. S6 at https://doi.org/10.5281/zenodo.8297777) using genomic features and regression models (146). The models employed were Superkingdom Bacteria regression models that take into consideration the common absence of 16S sequence and genome incompleteness in MAGs.

Phylogenetic and phylogenomic analyses of Zetaproteobacteria

Single-copy marker genes present in all genomes were detected and extracted using Anvio v.7.0 (121) with anvi-get-sequences-for-hmm-hits, using Anvio's Bacteria_71 and

GTDB's bac_120 collection of single-copy marker genes (139). Selection of marker genes was based on genes being present only in a single copy, found in at least 70% of all Zetaproteobacteria genomes, and supporting Zetaproteobacteria monophyly in individual marker phylogenetic trees (see Table S13 at https://doi.org/10.5281/zenodo.8297777). Selected marker genes were comparable to the amount of single-copy genes used for evolutionary placement of diversity within Zetaproteobacteria previously (40). Single-copy marker genes were manually checked, and phylogenetic trees of selected individual protein sequences constructed using ultrafast bootstrapping (147). Selected individual marker gene alignments were constructed using MAFFT L-INS-i v7.397 (148), trimmed with trimAl v1.4. rev15 with selected parameters -gt 0.5 -cons 60 (149), and concatenated using catfasta2phyml (https://github.com/nylander/catfasta2phyml). A maximum likelihood tree was constructed with IQ-TREE v2.0.3 (150) with non-parametric bootstrapping and using the best-fit model Q.pfam +F + I + I + R7 as determined by ModelFinder (151).

16S sequences were extracted using barrnap v.0.9 (https://github.com/tseemann/barrnap, settings: --kingdom 'bac' --evalue 1e-20), and only sequences longer than 500 bp were kept. The alignment was constructed using MAFFT L-INS-i v7.397 (148), manually inspected for non-matching sections, and trimmed with trimAl v1.4. rev15 with trimming option -gappyout (149). Using sequences of comparable length, a maximum likelihood tree of 16S sequences was constructed using IQ-TREE v2.0.3 (150) with non-parametric bootstrapping and the best-fit model GTR + F + I + I + R3 as determined by ModelFinder (151).

Functional annotation and genome comparison

Gene calling and functional annotation of MAGs were performed with an automated pipeline (152) conducting separate searches against Prokka v1.14 (153), NCBI COG (downloaded from NCBI webserver in February 2021), arCOG (version from 2018) (154), KEGG (downloaded in February 2021) (155), Pfam (release 33.0) (156), TIGRFAM (release 15.0) (157), CAZy (dbCAN v9) (158), Transporter Classification Database (downloaded from TCDB webserver in February 2021) (159), HydDB (downloaded from HydDB webserver in February 2021) (70), and NCBI_nr (downloaded from NCBI webserver in February 2021). Genes of interest (presence/absence) were determined for metabolic reconstruction mainly based on KEGG and TIGRFAM annotations (see Table S14 at https://doi.org/10.5281/zenodo.8297777), with the main functions discussed in the article manually inspected. Genes for CO_2 fixation pathways were screened using a customized script based on KEGG decoder v1.2.1 (160, 161). Iron oxidation genes were identified using FeGenie v1.1 tool (162), and manganese oxidation genes were annotated using MagicLamp v1.0 with curated lithotrophy hidden Markov models (HMMs) (84). Potential stalk formation gene homologs were identified based on a local BLAST together with previously studied sequences, % identity cutoffs, and average gene lengths previously defined (44). Metal resistance genes were identified in metagenome-resolved genomes and assembly using the BacMet database version 2.0 with experimentally confirmed and predicted resistance genes (163). Predicted resistance gene identification criterion of min. 85% sequence identity with the full-length coverage of the short reads (75–300+ bp) was used as advised by the database authors.

Codon bias expression prediction

Codon bias gene expression levels were predicted using coRdon R package (v 1.8.0, https://github.com/BioinfoHR/coRdon), based on the measure independent of length and composition (MILC) and MILC-based expression level predictor values (164).

Phylogenetic tree of Cyc2

Cyc2 sequences were identified in MAGs present in the black smoker iron microbial mat and in all Zetaproteobacteria from all sampled Fåvne sites using FeGenie (162).

Additional Cyc2 identifications were made from the top 10 hits using a blastp alignment based on the GenBank and NCBI_nr database. References were downloaded with BatchEntrez and reannotated as Cyc2 using FeGenie. Sequences shorter than 300 and longer than 600 amino acids were filtered out. Identical sequences were dereplicated using clustering with CD-HIT v4.8.1 (165). The resulting sequences of similar lengths were aligned using MAFFT L-INS-I v7.397 (148), manually checked in AliView v1.26 (166), and trimmed using trimAl v1.4. rev15 with -gt 0.7 (positions in the alignment with gaps in 30% or more of the sequences were removed) (149). A maximum likelihood phylogenetic tree was constructed with IQ-TREE v2.0.3 (150) using an alignment of 115 sequences with 388 positions and the best-fit model Q.pfam +F + I + I + R5, according to ModelFinder (151). Branch support values were calculated with standard bootstrapping with 1,000 iterations. The tree was rooted at midpoint.

Phylogenetic tree of Ni,Fe hydrogenase

The protein sequences of Ni,Fe large subunit hydrogenase 1d were identified from several sources: from the Fåvne iron microbial mat MAGs, the reference Zetaproteobacteria, along with their closest relatives. Closest relatives were identified by BLAST Diamond annotations using HydDB (downloaded from HydDB webserver in February 2021) (70), the top 50 hits using an additional blastp alignment using GenBank and nr database, and blastp using a JGI IMG database gene search at 85% identity threshold (August 2022). Also, 213 Ni,Fe large subunit hydrogenase 1d reference sequences from HydDB were added (downloaded from HydDB webserver in March 2021). Sequences shorter than 460 amino acids were filtered out. The resulting sequences of similar lengths were aligned using MAFFT L-INS-i v7.397 (148), manually checked in AliView v1.26 (166), and trimmed using trimAl v1.4. rev15 with -gt 0.5 -cons 60. A phylogenetic tree was constructed with IQ-TREE v2.0.3 (150) using an alignment of 317 sequences with 595 positions, based on maximum likelihood and the best-fit model LG + I + I + R7, according to ModelFinder (151). Branch support values were calculated with standard bootstrapping with 1,000 iterations. Redundant sequences from several sources (NCBI, IMG JGI) were pruned, leaving only one sequence representative. The tree was rooted at midpoint. Environment data were pulled from available metadata and taxonomy from NCBI with corrections based on GTDB where genomes were present.

Viral genomes

CheckV v.0.8.1 (167), VIBRANT v.1.2.1 (168), and DeepVirFinder (169) were used to search for viruses in the unbinned sequences. Quality of the viral genomes was checked using CheckV and reported according to minimum information requirements on uncultivated viral genomes (170). We predicted host-virus associations in the iron microbial mat using host CRISPR-spacers, integrated prophage, host tRNA genes, and k-mer signatures with VirMatcher, accessed in September 2022 (https://bitbucket.org/MAVERICLab/virmatcher/). This was done using minCED (v. 0.4.2; https://github.com/ctSkennerton/minced), BLAST (171), promiscuous tRNA sequences (172), tRNAscan (173), and WIsH (174). Score of 3 was used as a threshold value to assign hosts based on previous approaches (175). Host-virus pairs were analyzed also with PHP host predictor software using K-mer predictions (176).

ACKNOWLEDGMENTS

We thank the ROV Ægir6000 operator team and the R/V G.O. SARS crew for assistance during sampling, and Steffen L. Jørgensen for organizing the 2019 research cruise to the Fåvne vent field. We thank Irene Heggstad for assistance with scanning electron microscopy. The computations associated to taxonomic classification and annotation of genes were performed on resources provided by Sigma2—the National Infrastructure for High Performance Computing and Data Storage in Norway. We'd like to thank Roman A.

Barco for valuable suggestions during revision. We are grateful to the three anonymous reviewers for their thorough read-through and comments improving the manuscript.

This study is supported by the project DeepSeaQuence funded by the Norwegian Research Council (Grant No. 315427). The study received financial support from the Trond Mohn Foundation (Grant No. BFS2017TMT01) and the University of Bergen through the Centre for Deep Sea research (Grant No. TMS2020TMT13) and through the work packages "Biodiscovery and Bioprospecting" (R.S., I.H.S.) and "Diversity and Functioning of Hydrothermal Systems" (E.P.R.) of the former K. G. Jebsen Center for Deep Sea Research.

The authors declare that the research was conducted in the absence of any commercial or financial relationships that could be construed as a potential conflict of interest.

AUTHOR AFFILIATIONS

[1]Centre for Deep Sea Research, University of Bergen, Bergen, Norway
[2]Department of Earth Science, University of Bergen, Bergen, Norway
[3]Department of Biological Sciences, University of Bergen, Bergen, Norway
[4]Computational Biology Unit, University of Berge, Bergen, Norway

AUTHOR ORCIDs

Petra Hribovšek http://orcid.org/0000-0001-5668-9028
Emily Olesin Denny http://orcid.org/0000-0002-2729-3101
Håkon Dahle http://orcid.org/0000-0002-8308-3256
Achim Mall http://orcid.org/0000-0002-6681-2381
Thomas Øfstegaard Viflot http://orcid.org/0000-0001-6917-0954
Chanakan Boonnawa http://orcid.org/0009-0007-8574-076X
Eoghan P. Reeves http://orcid.org/0000-0003-0146-0714
Ida Helene Steen http://orcid.org/0000-0001-5903-6276
Runar Stokke http://orcid.org/0000-0002-6056-7119

AUTHOR CONTRIBUTIONS

Petra Hribovšek, Conceptualization, Data curation, Formal analysis, Investigation, Methodology, Visualization, Writing – original draft, Writing – review and editing | Emily Olesin Denny, Data curation, Writing – original draft | Håkon Dahle, Writing – original draft | Achim Mall, Data curation, Software, Writing – original draft | Thomas Øfstegaard Viflot, Formal analysis, Investigation, Writing – original draft | Chanakan Boonnawa, Conceptualization, Formal analysis, Funding acquisition, Investigation, Methodology, Supervision, Writing – original draft, Writing – review and editing | Eoghan P. Reeves, Conceptualization, Data curation, Formal analysis, Funding acquisition, Investigation, Methodology, Project administration, Supervision, Writing – original draft, Writing – review and editing | Ida Helene Steen, Conceptualization, Formal analysis, Funding acquisition, Investigation, Methodology, Supervision, Writing – original draft, Writing – review and editing | Runar Stokke, Conceptualization, Data curation, Formal analysis, Funding acquisition, Investigation, Methodology, Project administration, Supervision, Writing – original draft, Writing – review and editing

DATA AVAILABILITY

All MAGs in the study were deposited in NCBI, and accession numbers with associated BioProject and BioSamples with corresponding metadata are listed in Supplementary Material 1 Table S1 and Supplementary Material 2 Tables S2 and S4 at https://doi.org/10.5281/zenodo.8297777. Code used for the analyses is available at https://github.com/MicrobesGonnaMicrobe/Faavne_IronMats_Analysis.

REFERENCES

1. Kappler A, Bryce C, Mansor M, Lueder U, Byrne JM, Swanner ED. 2021. An evolving view on biogeochemical cycling of iron. Nat Rev Microbiol 19:360–374. https://doi.org/10.1038/s41579-020-00502-7
2. Rentz JA, Turner IP, Ullman JL. 2009. Removal of phosphorus from solution using biogenic iron oxides. Water Res 43:2029–2035. https://doi.org/10.1016/j.watres.2009.02.021
3. Bennett SA, Toner BM, Barco R, Edwards KJ. 2014. Carbon adsorption onto Fe oxyhydroxide stalks produced by a lithotrophic iron-oxidizing bacteria. Geobiology 12:146–156. https://doi.org/10.1111/gbi.12074
4. Sowers TD, Harrington JM, Polizzotto ML, Duckworth OW. 2017. Sorption of arsenic to biogenic iron (oxyhydr)oxides produced in circumneutral environments. Geochim Cosmochim Acta 198:194–207. https://doi.org/10.1016/j.gca.2016.10.049
5. Koschinsky A, Winkler A, Fritsche U. 2003. Importance of different types of marine particles for the scavenging of heavy metals in the deep-sea bottom water. Appl Geochem 18:693–710. https://doi.org/10.1016/S0883-2927(02)00161-0
6. Borch T, Kretzschmar R, Kappler A, Cappellen PV, Ginder-Vogel M, Voegelin A, Campbell K. 2010. Biogeochemical redox processes and their impact on contaminant dynamics. Environ Sci Technol 44:15–23. https://doi.org/10.1021/es9026248
7. McBeth JM, Little BJ, Ray RI, Farrar KM, Emerson D. 2011. Neutrophilic iron-oxidizing "Zetaproteobacteria" and mild steel corrosion in nearshore marine environments. Appl Environ Microbiol 77:1405–1412. https://doi.org/10.1128/AEM.02095-10
8. Emerson D. 2018. The role of iron-oxidizing bacteria in biocorrosion: a review. Biofouling 34:989–1000. https://doi.org/10.1080/08927014.2018.1526281
9. Braunschweig J, Bosch J, Meckenstock RU. 2013. Iron oxide nanoparticles in geomicrobiology: from biogeochemistry to bioremediation. N Biotechnol 30:793–802. https://doi.org/10.1016/j.nbt.2013.03.008
10. Rawlings DE, Johnson DB. 2007. The microbiology of biomining: development and optimization of mineral-oxidizing microbial consortia. Microbiology (Reading) 153:315–324. https://doi.org/10.1099/mic.0.2006/001206-0
11. Von Damm KL. 1990. Seafloor hydrothermal activity: black smoker chemistry and chimneys. Annu Rev Earth Planet Sci 18:173–204. https://doi.org/10.1146/annurev.ea.18.050190.001133
12. Mccollom TM. 2013. Observational, experimental, and theoretical constraints on carbon cycling in mid-ocean ridge hydrothermal systems, p 193–213. In Geophysical monograph series. American Geophysical Union (AGU). https://doi.org/10.1029/GM178
13. German CR, Seyfried WE. 2013. Hydrothermal processes, p 191–233. In Treatise geochemistry
14. Milesi V, Shock E, Seewald J, Trembath-Reichert E, Sylva SP, Huber JA, Lim DSS, German CR. 2023. Multiple parameters enable deconvolution of water-rock reaction paths in low-temperature vent fluids of the Kamaʻehuakanaloa (Lōʻihi) seamount. Geochim Cosmochim Acta 348:54–67. https://doi.org/10.1016/j.gca.2023.03.013
15. Amend JP, McCollom TM, Hentscher M, Bach W. 2011. Catabolic and anabolic energy for chemolithoautotrophs in deep-sea hydrothermal systems hosted in different rock types. Geochim Cosmochim Acta 75:5736–5748. https://doi.org/10.1016/j.gca.2011.07.041
16. Dahle H, Økland I, Thorseth IH, Pederesen RB, Steen IH. 2015. Energy landscapes shape microbial communities in hydrothermal systems on the Arctic Mid-Ocean Ridge. ISME J 9:1593–1606. https://doi.org/10.1038/ismej.2014.247
17. Dahle H, Le Moine Bauer S, Baumberger T, Stokke R, Pedersen RB, Thorseth IH, Steen IH. 2018. Energy landscapes in hydrothermal chimneys shape distributions of primary producers. Front Microbiol 9:1570. https://doi.org/10.3389/fmicb.2018.01570
18. Fleming EJ, Davis RE, McAllister SM, Chan CS, Moyer CL, Tebo BM, Emerson D. 2013. Hidden in plain sight: discovery of sheath-forming, iron-oxidizing Zetaproteobacteria at Loihi Seamount, Hawaii, USA. FEMS Microbiol Ecol 85:116–127. https://doi.org/10.1111/1574-6941.12104
19. Singer E, Heidelberg JF, Dhillon A, Edwards KJ. 2013. Metagenomic insights into the dominant Fe(II) oxidizing Zetaproteobacteria from an iron mat at Lōʻihi, Hawaiʻi. Front Microbiol 4:52. https://doi.org/10.3389/fmicb.2013.00052
20. Chan CS, McAllister SM, Leavitt AH, Glazer BT, Krepski ST, Emerson D. 2016. The architecture of iron microbial mats reflects the adaptation of chemolithotrophic iron oxidation in freshwater and marine environments. Front Microbiol 7:796. https://doi.org/10.3389/fmicb.2016.00796
21. McAllister SM, Vandzura R, Keffer JL, Polson SW, Chan CS. 2021. Aerobic and anaerobic iron oxidizers together drive denitrification and carbon cycling at marine iron-rich hydrothermal vents. ISME J 15:1271–1286. https://doi.org/10.1038/s41396-020-00849-y
22. Scott J.J, Glazer BT, Emerson D. 2017. Bringing microbial diversity into focus: high-resolution analysis of iron mats from the Lōʻihi Seamount. Environ Microbiol 19:301–316. https://doi.org/10.1111/1462-2920.13607
23. Sudek LA, Templeton AS, Tebo BM, Staudigel H. 2009. Microbial ecology of Fe (hydr)oxide mats and basaltic rock from Vailulu'U Seamount, American Samoa. Geomicrobiol J 26:581–596. https://doi.org/10.1080/01490450903263400
24. Scott JJ, Breier JA, Luther GW, Emerson D, Duperron S. 2015. Microbial iron mats at the mid-atlantic ridge and evidence that Zetaproteobacteria may be restricted to iron-oxidizing marine systems. PLoS One 10:e0119284. https://doi.org/10.1371/journal.pone.0119284
25. Astorch-Cardona A, Guerre M, Dolla A, Chavagnac V, Rommevaux C. 2023. Spatial comparison and temporal evolution of two marine iron-rich microbial mats from the lucky strike hydrothermal field, related to environmental variations. Front Mar Sci 10:115. https://doi.org/10.3389/fmars.2023.1038192
26. Kato S, Nakamura K, Toki T, Ishibashi J-I, Tsunogai U, Hirota A, Ohkuma M, Yamagishi A. 2012. Iron-based microbial ecosystem on and below the seafloor: a case study of hydrothermal fields of the Southern Mariana Trough. Front Microbiol 3:89. https://doi.org/10.3389/fmicb.2012.00089
27. Hager KW, Fullerton H, Butterfield DA, Moyer CL. 2017. Community structure of lithotrophically-driven hydrothermal microbial mats from the Mariana arc and back-arc. Front Microbiol 8:1578. https://doi.org/10.3389/fmicb.2017.01578
28. Makita H, Kikuchi S, Mitsunobu S, Takaki Y, Yamanaka T, Toki T, Noguchi T, Nakamura K, Abe M, Hirai M, Yamamoto M, Uematsu K, Miyazaki J, Nunoura T, Takahashi Y, Takai K. 2016. Comparative analysis of microbial communities in iron-dominated flocculent mats in deep-sea hydrothermal environments. Appl Environ Microbiol 82:5741–5755. https://doi.org/10.1128/AEM.01151-16
29. Davis RE, Moyer CL. 2008. Extreme spatial and temporal variability of hydrothermal microbial mat communities along the Mariana Island arc and Southern Mariana back-arc system. J Geophys Res 113:8–15. https://doi.org/10.1029/2007JB005413
30. Kato S, Kobayashi C, Kakegawa T, Yamagishi A. 2009. Microbial communities in iron-silica-rich microbial mats at deep-sea hydrothermal fields of the Southern Mariana Trough. Environ Microbiol 11:2094–2111. https://doi.org/10.1111/j.1462-2920.2009.01930.x
31. McAllister SM, Polson SW, Butterfield DA, Glazer BT, Sylvan JB, Chan CS. 2020. Validating the Cyc2 neutrophilic iron oxidation pathway using meta-omics of Zetaproteobacteria iron mats at marine hydrothermal vents. mSystems 5:e00553-19. https://doi.org/10.1128/mSystems.00553-19
32. Hodges TW, Olson JB. 2009. Molecular comparison of bacterial communities within iron-containing flocculent mats associated with submarine volcanoes along the Kermadec arc. Appl Environ Microbiol 75:1650–1657. https://doi.org/10.1128/AEM.01835-08
33. Forget NL, Murdock SA, Juniper SK. 2010. Bacterial diversity in Fe-rich hydrothermal sediments at two South Tonga arc submarine volcanoes. Geobiology 8:417–432. https://doi.org/10.1111/j.1472-4669.2010.00247.x
34. Breier JA, Gomez-Ibanez D, Reddington E, Huber JA, Emerson D. 2012. A precision multi-sampler for deep-sea hydrothermal microbial mat studies. Deep Sea Res Part I Oceanogr Res Pap 70:83–90. https://doi.org/10.1016/j.dsr.2012.10.006
35. Vander Roost J, Thorseth IH, Dahle H. 2017. Microbial analysis of Zetaproteobacteria and co-colonizers of iron mats in the troll wall vent

field, Arctic Mid-Ocean Ridge. PLoS One 12:e0185008. https://doi.org/10.1371/journal.pone.0185008
36. Vander Roost J, Daae FL, Steen IH, Thorseth IH, Dahle H. 2018. Distribution patterns of iron-oxidizing zeta- and beta-proteobacteria from different environmental settings at the Jan Mayen vent fields. Front Microbiol 9:3008. https://doi.org/10.3389/fmicb.2018.03008
37. Johannessen KC, Vander Roost J, Dahle H, Dundas SH, Pedersen RB, Thorseth IH. 2017. Environmental controls on biomineralization and Fe-mound formation in a low-temperature hydrothermal system at the Jan Mayen vent fields. Geochim Cosmochim Acta 202:101–123. https://doi.org/10.1016/j.gca.2016.12.016
38. Emerson D, Rentz JA, Lilburn TG, Davis RE, Aldrich H, Chan C, Moyer CL. 2007. A novel lineage of proteobacteria involved in formation of marine Fe-oxidizing microbial mat communities. PLoS One 2:e667. https://doi.org/10.1371/journal.pone.0000667
39. McAllister SM, Moore RM, Chan CS. 2018. Zetahunter, a reproducible taxonomic classification tool for tracking the ecology of the Zetaproteobacteria and other poorly resolved taxa. Microbiol Resour Announc 7:e00932-18. https://doi.org/10.1128/MRA.00932-18
40. McAllister SM, Moore RM, Gartman A, Luther GW, Emerson D, Chan CS. 2019. The Fe(II)-oxidizing Zetaproteobacteria: historical, ecological and genomic perspectives. FEMS Microbiol Ecol 95:fiz015. https://doi.org/10.1093/femsec/fiz015
41. Chiu BK, Kato S, McAllister SM, Field EK, Chan CS. 2017. Novel pelagic iron-oxidizing Zetaproteobacteria from the Chesapeake Bay oxic-anoxic transition zone. Front Microbiol 8:1280. https://doi.org/10.3389/fmicb.2017.01280
42. Emerson D, Scott JJ, Leavitt A, Fleming E, Moyer C. 2017. *In situ* estimates of iron-oxidation and accretion rates for iron-oxidizing bacterial mats at Lō'lhi Seamount. Deep Sea Res Part I Oceanogr Res Pap 126:31–39. https://doi.org/10.1016/j.dsr.2017.05.011
43. Chan CS, Fakra SC, Emerson D, Fleming EJ, Edwards KJ. 2011. Lithotrophic iron-oxidizing bacteria produce organic stalks to control mineral growth: implications for biosignature formation. ISME J 5:717–727. https://doi.org/10.1038/ismej.2010.173
44. Koeksoy E, Bezuidt OM, Bayer T, Chan CS, Emerson D. 2021. Zetaproteobacteria pan-genome reveals candidate gene cluster for twisted stalk biosynthesis and export. Front Microbiol 12:679409. https://doi.org/10.3389/fmicb.2021.679409
45. Kato S, Ohkuma M, Powell DH, Krepski ST, Oshima K, Hattori M, Shapiro N, Woyke T, Chan CS. 2015. Comparative genomic insights into ecophysiology of neutrophilic, microaerophilic iron oxidizing bacteria. Front Microbiol 6:1265. https://doi.org/10.3389/fmicb.2015.01265
46. Makita H, Tanaka E, Mitsunobu S, Miyazaki M, Nunoura T, Uematsu K, Takaki Y, Nishi S, Shimamura S, Takai K. 2017. Mariprofundus micogutta sp. nov., a novel iron-oxidizing zetaproteobacterium isolated from a deep-sea hydrothermal field at the Bayonnaise knoll of the Izu-Ogasawara arc, and a description of Mariprofundales ord. nov. and Zetaproteobacteria classis nov. Arch Microbiol 199:335–346. https://doi.org/10.1007/s00203-016-1307-4
47. Emerson D, Moyer CL. 2002. Neutrophilic Fe-oxidizing bacteria are abundant at the Loihi Seamount hydrothermal vents and play a major role in Fe oxide deposition. Appl Environ Microbiol 68:3085–3093. https://doi.org/10.1128/AEM.68.6.3085-3093.2002
48. Field EK, Sczyrba A, Lyman AE, Harris CC, Woyke T, Stepanauskas R, Emerson D. 2015. Genomic insights into the uncultivated marine Zetaproteobacteria at Loihi Seamount. ISME J 9:857–870. https://doi.org/10.1038/ismej.2014.183
49. Garrison CE, Price KA, Field EK. 2019. Environmental evidence for and genomic insight into the preference of iron-oxidizing bacteria for more-corrosion-resistant stainless steel at higher salinities. Appl Environ Microbiol 85:1–14. https://doi.org/10.1128/AEM.00483-19
50. Barco RA, Emerson D, Sylvan JB, Orcutt BN, Jacobson Meyers ME, Ramírez GA, Zhong JD, Edwards KJ. 2015. New insight into microbial iron oxidation as revealed by the proteomic profile of an obligate iron-oxidizing chemolithoautotroph. Appl Environ Microbiol 81:5927–5937. https://doi.org/10.1128/AEM.01374-15
51. Keffer JL, McAllister SM, Garber AI, Hallahan BJ, Sutherland MC, Rozovsky S, Chan CS. 2021. Iron oxidation by a fused cytochrome-porin common to diverse iron-oxidizing bacteria. mBio 12:e0107421. https://doi.org/10.1128/mBio.01074-21
52. He S, Barco RA, Emerson D, Roden EE. 2017. Comparative genomic analysis of neutrophilic iron(II) oxidizer genomes for candidate genes in extracellular electron transfer. Front Microbiol 8:1584. https://doi.org/10.3389/fmicb.2017.01584
53. Mori JF, Scott JJ, Hager KW, Moyer CL, Küsel K, Emerson D. 2017. Physiological and ecological implications of an iron- or hydrogen-oxidizing member of the Zetaproteobacteria, *Ghiorsea* bivora, gen. nov., sp. nov. ISME J 11:2624–2636. https://doi.org/10.1038/ismej.2017.132
54. Gini C, Jamieson JW, Robert K, Barreyre T, Reeves EP, Gartman A, Jorgensen SL. 2022. Iron oxide- and oxyhydroxide-rich hydrothermal deposits at the Fåvne vent field on the Ultraslow mohns mid-ocean ridge. Abstr. OS45D-1226. AGU Fall Meeting 2022. Chicago, IL
55. Boonnawa C, Viflot Øftsegaard T, Pereira SI, Barreyre T, Jamieson JW, Stokke R, Steen IH, Scheffler J, Meckel E-M, Rosner M, Fiebig J, Reeves EP. 2022. Diverse styles of hydrothermal chemistry on the Ultraslow Arctic mohns ridge: the Fåvne, Ægir and Loki's castle vent fields. Abstr. OS55B-02. AGU Fall Meeting 2022. Chicago, IL
56. Sahlström F, Strmić Palinkaš S, Hjorth Dundas S, Sendula E, Cheng Y, Wold M, Pedersen RB. 2023. Mineralogical distribution and genetic aspects of cobalt at the active Fåvne and Loki's castle Seafloor massive sulfide deposits, Arctic Mid-Ocean Ridges. Ore Geol Rev 153:105261. https://doi.org/10.1016/j.oregeorev.2022.105261
57. Charlou JL, Donval JP, Konn C, Ondréas H, Fouquet Y, Jean-Baptiste P, Fourré E. 2013. High production and fluxes of H2 and CH4 and evidence of abiotic hydrocarbon synthesis by serpentinization in ultramafic-hosted hydrothermal systems on the mid-atlantic ridge, p 265–296. In Diversity of hydrothermal systems on slow spreading ocean ridges. American Geophysical Union (AGU). https://doi.org/10.1029/GM188
58. Urich T, Lanzén A, Stokke R, Pedersen RB, Bayer C, Thorseth IH, Schleper C, Steen IH, Ovreas L. 2014. Microbial community structure and functioning in marine sediments associated with diffuse hydrothermal venting assessed by integrated meta-omics. Environ Microbiol 16:2699–2710. https://doi.org/10.1111/1462-2920.12283
59. Dahle H, Roalkvam I, Thorseth IH, Pedersen RB, Steen IH. 2013. The versatile *in situ* gene expression of an Epsilonproteobacteria-dominated biofilm from a hydrothermal chimney. Environ Microbiol Rep 5:282–290. https://doi.org/10.1111/1758-2229.12016
60. Stokke R, Dahle H, Roalkvam I, Wissuwa J, Daae FL, Tooming-Klunderud A, Thorseth IH, Pedersen RB, Steen IH. 2015. Functional interactions among filamentous Epsilonproteobacteria and Bacteroidetes in a deep-sea hydrothermal vent biofilm. Environ Microbiol 17:4063–4077. https://doi.org/10.1111/1462-2920.12970
61. Steen IH, Dahle H, Stokke R, Roalkvam I, Daae F-L, Rapp HT, Pedersen RB, Thorseth IH. 2015. Novel barite chimneys at the Loki's castle vent field shed light on key factors shaping microbial communities and functions in hydrothermal systems. Front Microbiol 6:1510. https://doi.org/10.3389/fmicb.2015.01510
62. Dick GJ. 2019. The microbiomes of deep-sea hydrothermal vents: distributed globally, shaped locally. Nat Rev Microbiol 17:271–283. https://doi.org/10.1038/s41579-019-0160-2
63. Waite DW, Vanwonterghem I, Rinke C, Parks DH, Zhang Y, Takai K, Sievert SM, Simon J, Campbell BJ, Hanson TE, Woyke T, Klotz MG, Hugenholtz P. 2018. Addendum: comparative genomic analysis of the class *Epsilonproteobacteria* and proposed reclassification to Epsilonbacteraeota (phyl. nov.). Front Microbiol 9:772. https://doi.org/10.3389/fmicb.2018.00772
64. Bowers RM, Kyrpides NC, Stepanauskas R, Harmon-Smith M, Doud D, Reddy TBK, Schulz F, Jarett J, Rivers AR, Eloe-Fadrosh EA, et al. 2017. Minimum information about a single amplified genome (MISAG) and a metagenome-assembled genome (MIMAG) of bacteria and archaea. Nat Biotechnol 35:725–731. https://doi.org/10.1038/nbt.3893
65. Jain C, Rodriguez-R LM, Phillippy AM, Konstantinidis KT, Aluru S. 2018. High throughput ANI analysis of 90K prokaryotic genomes reveals clear species boundaries. Nat Commun 9:5114. https://doi.org/10.1038/s41467-018-07641-9
66. Chun J, Oren A, Ventosa A, Christensen H, Arahal DR, da Costa MS, Rooney AP, Yi H, Xu X-W, De Meyer S, Trujillo ME. 2018. Proposed minimal standards for the use of genome data for the taxonomy of prokaryotes. Int J Syst Evol Microbiol 68:461–466. https://doi.org/10.1099/ijsem.0.002516

67. Cambon-Bonavita M-A, Aubé J, Cueff-Gauchard V, Reveillaud J. 2021. Niche partitioning in the Rimicaris exoculata holobiont: the case of the first symbiotic Zetaproteobacteria. Microbiome 9:87. https://doi.org/10.1186/s40168-021-01045-6
68. Tully BJ, Wheat CG, Glazer BT, Huber JA. 2018. A dynamic microbial community with high functional redundancy inhabits the cold, oxic subseafloor aquifer. ISME J 12:1–16. https://doi.org/10.1038/ismej.2017.187
69. Konstantinidis KT, Rosselló-Móra R, Amann R. 2017. Uncultivated microbes in need of their own taxonomy. ISME J 11:2399–2406. https://doi.org/10.1038/ismej.2017.113
70. Søndergaard D, Pedersen CNS, Greening C. 2016. HydDB: a web tool for hydrogenase classification and analysis. Sci Rep 6:34212. https://doi.org/10.1038/srep34212
71. Castelle C, Guiral M, Malarte G, Ledgham F, Leroy G, Brugna M, Giudici-Orticoni MT. 2008. A new iron-oxidizing/O2-reducing supercomplex spanning both inner and outer membranes, isolated from the extreme acidophile Acidithiobacillus ferrooxidans. J Biol Chem 283:25803–25811. https://doi.org/10.1074/jbc.M802496200
72. Jeans C, Singer SW, Chan CS, Verberkmoes NC, Shah M, Hettich RL, Banfield JF, Thelen MP. 2008. Cytochrome 572 is a conspicuous membrane protein with iron oxidation activity purified directly from a natural acidophilic microbial community. ISME J 2:542–550. https://doi.org/10.1038/ismej.2008.17
73. Pester NJ, Rough M, Ding K, Seyfried WE. 2011. A new Fe/Mn geothermometer for hydrothermal systems: implications for high-salinity fluids at 13°N on the East Pacific rise. Geochim Cosmochim Acta 75:7881–7892. https://doi.org/10.1016/j.gca.2011.08.043
74. Geszvain K, McCarthy JK, Tebo BM. 2013. Elimination of manganese(II, III) oxidation in *Pseudomonas putida* GB-1 by a double knockout of two putative multicopper oxidase genes. Appl Environ Microbiol 79:357–366. https://doi.org/10.1128/AEM.01850-12
75. Anderson CR, Davis RE, Bandolin NS, Baptista AM, Tebo BM. 2011. Analysis of *in situ* manganese(II) oxidation in the Columbia river and offshore plume: linking aurantimonas and the associated microbial community to an active biogeochemical cycle. Environ Microbiol 13:1561–1576. https://doi.org/10.1111/j.1462-2920.2011.02462.x
76. Anderson CR, Johnson HA, Caputo N, Davis RE, Torpey JW, Tebo BM. 2009. Mn(II) oxidation is catalyzed by heme peroxidases in "Aurantimonas manganoxydans" strain SI85-9A1 and Erythrobacter sp. strain SD-21. Appl Environ Microbiol 75:4130–4138. https://doi.org/10.1128/AEM.02890-08
77. Ridge JP, Lin M, Larsen EI, Fegan M, McEwan AG, Sly LI. 2007. A multicopper oxidase is essential for manganese oxidation and laccase-like activity in Pedomicrobium sp. ACM 3067. Environ Microbiol 9:944–953. https://doi.org/10.1111/j.1462-2920.2006.01216.x
78. Larsen EI, Sly LI, McEwan AG. 1999. Manganese(II) adsorption and oxidation by whole cells and a membrane fraction of Pedomicrobium sp. ACM 3067. Arch Microbiol 171:257–264. https://doi.org/10.1007/s002030050708
79. Kulajta C, Thumfart JO, Haid S, Daldal F, Koch HG. 2006. Multi-step assembly pathway of the cbb3-type cytochrome c oxidase complex. J Mol Biol 355:989–1004. https://doi.org/10.1016/j.jmb.2005.11.039
80. Jain A, Gralnick JA. 2020. Evidence for auxiliary anaerobic metabolism in obligately aerobic Zetaproteobacteria. ISME J 14:1057–1062. https://doi.org/10.1038/s41396-020-0586-6
81. Berg IA. 2011. Ecological aspects of the distribution of different autotrophic CO2 fixation pathways. Appl Environ Microbiol 77:1925–1936. https://doi.org/10.1128/AEM.02473-10
82. Garritano AN, Song W, Thomas T. 2022. Carbon fixation pathways across the bacterial and archaeal tree of life. PNAS Nexus 1:gac226. https://doi.org/10.1093/pnasnexus/pgac226
83. Sánchez-Andrea I, Guedes IA, Hornung B, Boeren S, Lawson CE, Sousa DZ, Bar-Even A, Claassens NJ, Stams AJM. 2020. The reductive glycine pathway allows autotrophic growth of Desulfovibrio desulfuricans. Nat Commun 11:5090. https://doi.org/10.1038/s41467-020-18906-7
84. Garber AI, Ramirez GA, Merino N, Pavia MJ, McAllister SM. 2020. GitHub repository. MagicLamp: toolkit for annotation of 'omics datasets using curated HMM sets. Available from: https://github.com/Arkadiy-Garber/MagicLamp
85. Barco RA, Hoffman CL, Ramírez GA, Toner BM, Edwards KJ, Sylvan JB. 2017. *In-situ* incubation of iron-sulfur mineral reveals a diverse chemolithoautotrophic community and a new biogeochemical role for Thiomicrospira. Environ Microbiol 19:1322–1337. https://doi.org/10.1111/1462-2920.13666
86. Henri PA, Rommevaux-Jestin C, Lesongeur F, Mumford A, Emerson D, Godfroy A, Ménez B. 2015. Structural iron (II) of basaltic glass as an energy source for Zetaproteobacteria in an abyssal plain environment, off the mid atlantic ridge. Front Microbiol 6:1518. https://doi.org/10.3389/fmicb.2015.01518
87. McDermott JM, Sylva SP, Ono S, German CR, Seewald JS. 2020. Abiotic redox reactions in hydrothermal mixing zones: decreased energy availability for the subsurface biosphere. Proc Natl Acad Sci U S A 117:20453–20461. https://doi.org/10.1073/pnas.2003108117
88. Duchinski K, Moyer CL, Hager K, Fullerton H. 2019. Fine-scale biogeography and the inference of ecological interactions among neutrophilic iron-oxidizing Zetaproteobacteria as determined by a rule-based microbial network. Front. Microbiol 10:2389. https://doi.org/10.3389/fmicb.2019.02389
89. McAllister SM, Davis RE, McBeth JM, Tebo BM, Emerson D, Moyer CL. 2011. Biodiversity and emerging biogeography of the neutrophilic iron-oxidizing Zetaproteobacteria. Appl Environ Microbiol 77:5445–5457. https://doi.org/10.1128/AEM.00533-11
90. Little CTS, Johannessen KC, Bengtson S, Chan CS, Ivarsson M, Slack JF, Broman C, Thorseth IH, Grenne T, Rouxel OJ, Bekker A. 2021. A late Paleoproterozoic (1.74 Ga) deep-sea, low-temperature, iron-oxidizing microbial hydrothermal vent community from Arizona, USA. Geobiology 19:228–249. https://doi.org/10.1111/gbi.12434
91. Chan CS, Emerson D, Luther GW. 2016. The role of microaerophilic Fe-oxidizing micro-organisms in producing banded iron formations. Geobiology 14:509–528. https://doi.org/10.1111/gbi.12192
92. Dreher CL, Schad M, Robbins LJ, Konhauser KO, Kappler A, Joshi P. 2021. Microbial processes during deposition and diagenesis of banded iron formations. PalZ 95:593–610. https://doi.org/10.1007/s12542-021-00598-z
93. Toner BM, Berquó TS, Michel FM, Sorensen JV, Templeton AS, Edwards KJ. 2012. Mineralogy of iron microbial mats from Loihi Seamount. Front Microbiol 3:118. https://doi.org/10.3389/fmicb.2012.00118
94. Banfield JF, Moreau JW, Chan CS, Welch SA, Little B. 2001. Mineralogical biosignatures and the search for life on Mars. Astrobiology 1:447–465. https://doi.org/10.1089/153110701753593856
95. Beam JP, Scott JJ, McAllister SM, Chan CS, McManus J, Meysman FJR, Emerson D. 2018. Biological rejuvenation of iron oxides in bioturbated marine sediments. ISME J 12:1389–1394. https://doi.org/10.1038/s41396-017-0032-6
96. Emerson D, Moyer CL. 2010. Microbiology of seamounts: common patterns observed in community structure. Oceanog 23:148–163. https://doi.org/10.5670/oceanog.2010.67
97. Edwards KJ, Rogers DR, Wirsen CO, McCollom TM. 2003. Isolation and characterization of novel psychrophilic, neutrophilic, Fe-oxidizing, chemolithoautotrophic alpha- and gamma-proteobacteria from the deep sea. Appl Environ Microbiol 69:2906–2913. https://doi.org/10.1128/AEM.69.5.2906-2913.2003
98. Zhong Y-W, Zhou P, Cheng H, Zhou Y-D, Pan J, Xu L, Li M, Tao C-H, Wu Y-H, Xu X-W. 2022. Metagenomic features characterized with microbial iron oxidoreduction and mineral interaction in Southwest Indian ridge. Microbiol Spectr 10:e0061422. https://doi.org/10.1128/spectrum.00614-22
99. Carlson HK, Clark IC, Melnyk RA, Coates JD. 2012. Toward a mechanistic understanding of anaerobic nitrate-dependent iron oxidation: balancing electron uptake and detoxification. Front Microbiol 3:57. https://doi.org/10.3389/fmicb.2012.00057
100. Fullerton H, Hager KW, McAllister SM, Moyer CL. 2017. Hidden diversity revealed by genome-resolved metagenomics of iron-oxidizing microbial mats from Lō'ihi Seamount, Hawai'I. ISME J 11:1900–1914. https://doi.org/10.1038/ismej.2017.40
101. Blackwell N, Bryce C, Straub D, Kappler A, Kleindienst S. 2020. Genomic insights into two novel Fe(II)-oxidizing Zetaproteobacteria isolates reveal lifestyle adaption to coastal marine sediments. Appl Environ Microbiol 86:e01160-20. https://doi.org/10.1128/AEM.01160-20

102. Tabita FR, Satagopan S, Hanson TE, Kreel NE, Scott SS. 2008. Distinct form I, II, III, and IV Rubisco proteins from the three kingdoms of life provide clues about Rubisco evolution and structure/function relationships. J Exp Bot 59:1515–1524. https://doi.org/10.1093/jxb/erm361
103. Badger MR, Bek EJ. 2008. Multiple Rubisco forms in proteobacteria: their functional significance in relation to CO2 acquisition by the CBB cycle. J Exp Bot 59:1525–1541. https://doi.org/10.1093/jxb/erm297
104. Singer E, Emerson D, Webb EA, Barco RA, Kuenen JG, Nelson WC, Chan CS, Comolli LR, Ferriera S, Johnson J, Heidelberg JF, Edwards KJ. 2011. Mariprofundus ferrooxydans PV-1 the first genome of a marine Fe(II) oxidizing Zetaproteobacterium. PLoS One 6:e25386. https://doi.org/10.1371/journal.pone.0025386
105. Mumford AC, Adaktylou IJ, Emerson D. 2016. Peeking under the iron curtain: development of a microcosm for imaging the colonization of steel surfaces by Mariprofundus sp. strain DIS-1, an oxygen-tolerant Fe-oxidizing bacterium. Appl Environ Microbiol 82:6799–6807. https://doi.org/10.1128/AEM.01990-16
106. McDermott JM, Sylva SP, Ono S, German CR, Seewald JS. 2018. Geochemistry of fluids from earth's deepest ridge-crest hot-springs: piccard hydrothermal field, Mid-Cayman Rise. Geochim Cosmochim Acta 228:95–118. https://doi.org/10.1016/j.gca.2018.01.021
107. Charlou JL, Donval JP, Fouquet Y, Jean-Baptiste P, Holm N. 2002. Geochemistry of high H2 and CH4 vent fluids issuing from ultramafic rocks at the Rainbow hydrothermal field (36°14′N,MAR). Chem Geol 191:345–359. https://doi.org/10.1016/S0009-2541(02)00134-1
108. Schrenk MO, Kelley DS, Delaney JR, Baross JA. 2003. Incidence and diversity of microorganisms within the walls of an active deep-sea sulfide chimney. Appl Environ Microbiol 69:3580–3592. https://doi.org/10.1128/AEM.69.6.3580-3592.2003
109. Seewald JS, Doherty KW, Hammar TR, Liberatore SP. 2002. A new gas-tight isobaric sampler for hydrothermal fluids. Deep Sea Res Part I Oceanogr Res Pap 49:189–196. https://doi.org/10.1016/S0967-0637(01)00046-2
110. Laso-Pérez R, Krukenberg V, Musat F, Wegener G. 2018. Establishing anaerobic hydrocarbon-degrading enrichment cultures of microorganisms under strictly anoxic conditions. Nat Protoc 13:1310–1330. https://doi.org/10.1038/nprot.2018.030
111. Glöckner FO, Amann R, Alfreider A, Pernthaler J, Psenner R, Trebesius K, Schleifer KH. 1996. An *in situ* hybridization protocol for detection and identification of planktonic bacteria. Syst Appl Microbiol 19:403–406. https://doi.org/10.1016/S0723-2020(96)80069-5
112. Wallner G, Amann R, Beisker W. 1993. Optimizing fluorescent *in situ* hybridization with rRNA - targeted oligonucleotide probes for flow cytometric identification of microorganisms. Cytometry 14:136–143. https://doi.org/10.1002/cyto.990140205
113. De Coster W, D'Hert S, Schultz DT, Cruts M, Van Broeckhoven C. 2018. Nanopack: visualizing and processing long-read sequencing data. Bioinformatics 34:2666–2669. https://doi.org/10.1093/bioinformatics/bty149
114. Ewels P, Magnusson M, Lundin S, Käller M. 2016. MultiQC: summarize analysis results for multiple tools and samples in a single report. Bioinformatics 32:3047–3048. https://doi.org/10.1093/bioinformatics/btw354
115. Minoche AE, Dohm JC, Himmelbauer H. 2011. Evaluation of genomic high-throughput sequencing data generated on Illumina HiSeq and genome analyzer systems. Genome Biol 12:R112. https://doi.org/10.1186/gb-2011-12-11-r112
116. Eren AM, Vineis JH, Morrison HG, Sogin ML, Jordan IK. 2013. A filtering method to generate high quality short reads using Illumina paired-end technology. PLoS One 8:e66643. https://doi.org/10.1371/journal.pone.0066643
117. Bushnell B, Rood J, Singer E. 2017. Bbmerge - accurate paired shotgun read merging via overlap. PLoS One 12:e0185056. https://doi.org/10.1371/journal.pone.0185056
118. Li D, Liu CM, Luo R, Sadakane K, Lam TW. 2015. MEGAHIT: an ultra-fast single-node solution for large and complex metagenomics assembly via succinct de Bruijn graph. Bioinformatics 31:1674–1676. https://doi.org/10.1093/bioinformatics/btv033
119. Langmead B, Salzberg SL. 2012. Fast gapped-read alignment with Bowtie 2. Nat Methods 9:357–359. https://doi.org/10.1038/nmeth.1923
120. Li H, Handsaker B, Wysoker A, Fennell T, Ruan J, Homer N, Marth G, Abecasis G, Durbin R, 1000 Genome Project Data Processing Subgroup. 2009. The sequence alignment/map format and SAMtools. Bioinformatics 25:2078–2079. https://doi.org/10.1093/bioinformatics/btp352
121. Eren AM, Esen ÖC, Quince C, Vineis JH, Morrison HG, Sogin ML, Delmont TO. 2015. Anvi'o: an advanced analysis and visualization platform for 'omics data. PeerJ 3:e1319. https://doi.org/10.7717/peerj.1319
122. Ruan J, Li H. 2020. Fast and accurate long-read assembly with wtdbg2. Nat Methods 17:155–158. https://doi.org/10.1038/s41592-019-0669-3
123. Vaser R, Sović I, Nagarajan N, Šikić M. 2017. Fast and accurate *de novo* genome assembly from long uncorrected reads. Genome Res 27:737–746. https://doi.org/10.1101/gr.214270.116
124. Alneberg J, Bjarnason BS, de Bruijn I, Schirmer M, Quick J, Ijaz UZ, Lahti L, Loman NJ, Andersson AF, Quince C. 2014. Binning metagenomic contigs by coverage and composition. Nat Methods 11:1144–1146. https://doi.org/10.1038/nmeth.3103
125. Kang DD, Froula J, Egan R, Wang Z. 2015. MetaBAT, an efficient tool for accurately reconstructing single genomes from complex microbial communities. PeerJ 3:e1165. https://doi.org/10.7717/peerj.1165
126. Kang DD, Li F, Kirton E, Thomas A, Egan R, An H, Wang Z. 2019. MetaBAT 2: an adaptive binning algorithm for robust and efficient genome reconstruction from metagenome assemblies. PeerJ 7:e7359. https://doi.org/10.7717/peerj.7359
127. Sieber CMK, Probst AJ, Sharrar A, Thomas BC, Hess M, Tringe SG, Banfield JF. 2018. Recovery of genomes from metagenomes via a dereplication, aggregation and scoring strategy. Nat Microbiol 3:836–843. https://doi.org/10.1038/s41564-018-0171-1
128. Nurk S, Meleshko D, Korobeynikov A, Pevzner PA. 2017. MetaSPAdes: a new versatile metagenomic assembler. Genome Res 27:824–834. https://doi.org/10.1101/gr.213959.116
129. Mikheenko A, Saveliev V, Gurevich A. 2016. MetaQUAST: evaluation of metagenome assemblies. Bioinformatics 32:1088–1090. https://doi.org/10.1093/bioinformatics/btv697
130. Kolmogorov M, Bickhart DM, Behsaz B, Gurevich A, Rayko M, Shin SB, Kuhn K, Yuan J, Polevikov E, Smith TPL, Pevzner PA. 2020. metaFlye: scalable long-read metagenome assembly using repeat graphs. Nat Methods 17:1103–1110. https://doi.org/10.1038/s41592-020-00971-x
131. Walker BJ, Abeel T, Shea T, Priest M, Abouelliel A, Sakthikumar S, Cuomo CA, Zeng Q, Wortman J, Young SK, Earl AM. 2014. Pilon: an integrated tool for comprehensive microbial variant detection and genome assembly improvement. PLoS One 9:e112963. https://doi.org/10.1371/journal.pone.0112963
132. Li H, Durbin R. 2009. Fast and accurate short read alignment with burrows-wheeler transform. Bioinformatics 25:1754–1760. https://doi.org/10.1093/bioinformatics/btp324
133. Li Heng, Birol I. 2018. Minimap2: pairwise alignment for nucleotide sequences. Bioinformatics 34:3094–3100. https://doi.org/10.1093/bioinformatics/bty191
134. Uritskiy GV, DiRuggiero J, Taylor J. 2018. MetaWRAP-a flexible pipeline for genome-resolved metagenomic data analysis. Microbiome 6:158. https://doi.org/10.1186/s40168-018-0541-1
135. Wu Y-W, Simmons BA, Singer SW. 2016. MaxBin 2.0: an automated binning algorithm to recover genomes from multiple metagenomic datasets. Bioinformatics 32:605–607. https://doi.org/10.1093/bioinformatics/btv638
136. Parks DH, Imelfort M, Skennerton CT, Hugenholtz P, Tyson GW. 2015. CheckM: assessing the quality of microbial genomes recovered from isolates, single cells, and metagenomes. Genome Res 25:1043–1055. https://doi.org/10.1101/gr.186072.114
137. Chklovski A, Parks DH, Woodcroft BJ, Tyson GW. 2022. CheckM2: a rapid, scalable and accurate tool for assessing microbial genome quality using machine learning. Bioinformatics (Oxford, England). https://doi.org/10.1101/2022.07.11.499243
138. Olm MR, Brown CT, Brooks B, Banfield JF. 2017. DRep: a tool for fast and accurate genomic comparisons that enables improved genome recovery from metagenomes through de-replication. ISME J 11:2864–2868. https://doi.org/10.1038/ismej.2017.126
139. Chaumeil P-A, Mussig AJ, Hugenholtz P, Parks DH, Hancock J. 2020. GTDB-Tk: a toolkit to classify genomes with the genome taxonomy database. Bioinformatics 36:1925–1927. https://doi.org/10.1093/bioinformatics/btz848
140. Gruber-Vodicka HR, Seah BKB, Pruesse E, Arumugam M, Kato S. 2020. phyloFlash: rapid small-subunit rRNA profiling and targeted assembly from metagenomes. mSystems 5:e00920-20. https://doi.org/10.1128/mSystems.00920-20

141. Nayfach S, Roux S, Seshadri R, Udwary D, Varghese N, Schulz F, Wu D, Paez-Espino D, Chen I-M, Huntemann M, et al. 2021. A genomic catalog of earth's microbiomes. Nat Biotechnol 39:499–509. https://doi.org/10.1038/s41587-020-0718-6
142. Seyler LM, Trembath-Reichert E, Tully BJ, Huber JA. 2021. Time-series transcriptomics from cold, oxic subseafloor crustal fluids reveals a motile, mixotrophic microbial community. ISME J 15:1192–1206. https://doi.org/10.1038/s41396-020-00843-4
143. Konstantinidis KT, Tiedje JM. 2005. Towards a genome-based taxonomy for prokaryotes. J Bacteriol 187:6258–6264. https://doi.org/10.1128/JB.187.18.6258-6264.2005
144. Varghese NJ, Mukherjee S, Ivanova N, Konstantinidis KT, Mavrommatis K, Kyrpides NC, Pati A. 2015. Microbial species delineation using whole genome sequences. Nucleic Acids Res 43:6761–6771. https://doi.org/10.1093/nar/gkv657
145. Kim D, Park S, Chun J. 2021. Introducing EzAAI: a pipeline for high throughput calculations of prokaryotic average amino acid identity. J Microbiol 59:476–480. https://doi.org/10.1007/s12275-021-1154-0
146. Sauer DB, Wang DN. 2019. Predicting the optimal growth temperatures of prokaryotes using only genome derived features. Bioinformatics 35:3224–3231. https://doi.org/10.1093/bioinformatics/btz059
147. Minh BQ, Nguyen MAT, von Haeseler A. 2013. Ultrafast approximation for phylogenetic bootstrap. Mol Biol Evol 30:1188–1195. https://doi.org/10.1093/molbev/mst024
148. Katoh K, Standley DM. 2013. MAFFT multiple sequence alignment software version 7: improvements in performance and usability. Mol Biol Evol 30:772–780. https://doi.org/10.1093/molbev/mst010
149. Capella-Gutiérrez S, Silla-Martínez JM, Gabaldón T. 2009. trimAl: a tool for automated alignment trimming in large-scale phylogenetic analyses. Bioinformatics 25:1972–1973. https://doi.org/10.1093/bioinformatics/btp348
150. Nguyen L-T, Schmidt HA, von Haeseler A, Minh BQ. 2015. IQ-TREE: a fast and effective stochastic algorithm for estimating maximum-likelihood phylogenies. Mol Biol Evol 32:268–274. https://doi.org/10.1093/molbev/msu300
151. Kalyaanamoorthy S, Minh BQ, Wong TKF, von Haeseler A, Jermiin LS. 2017. ModelFinder: fast model selection for accurate phylogenetic estimates. Nat Methods 14:587–589. https://doi.org/10.1038/nmeth.4285
152. Dombrowski N, Williams TA, Sun J, Woodcroft BJ, Lee J-H, Minh BQ, Rinke C, Spang A. 2020. Undinarchaeota illuminate DPANN phylogeny and the impact of gene transfer on archaeal evolution. Nat Commun 11:3939. https://doi.org/10.1038/s41467-020-17408-w
153. Seemann T. 2014. Prokka: rapid prokaryotic genome annotation. Bioinformatics 30:2068–2069. https://doi.org/10.1093/bioinformatics/btu153
154. Makarova KS, Wolf YI, Koonin EV. 2015. Archaeal clusters of orthologous genes (arCOGs): an update and application for analysis of shared features between thermococcales, methanococcales, and methanobacteriales. Life (Basel) 5:818–840. https://doi.org/10.3390/life5010818
155. Aramaki T, Blanc-Mathieu R, Endo H, Ohkubo K, Kanehisa M, Goto S, Ogata H. 2020. KofamKOALA: KEGG ortholog assignment based on profile HMM and adaptive score threshold. Bioinformatics 36:2251–2252. https://doi.org/10.1093/bioinformatics/btz859
156. Bateman A, Coin L, Durbin R, Finn RD, Hollich V, Griffiths-Jones S, Khanna A, Marshall M, Moxon S, Sonnhammer ELL, Studholme DJ, Yeats C, Eddy SR. 2004. The Pfam protein families database. Nucleic Acids Res 32:D138–41. https://doi.org/10.1093/nar/gkh121
157. Haft DH, Selengut JD, White O. 2003. The TIGRFAMs database of protein families. Nucleic Acids Res 31:371–373. https://doi.org/10.1093/nar/gkg128
158. Cantarel BL, Coutinho PM, Rancurel C, Bernard T, Lombard V, Henrissat B. 2009. The carbohydrate-active EnZymes database (CAZy): an expert resource for glycogenomics. Nucleic Acids Res 37:D233–8. https://doi.org/10.1093/nar/gkn663
159. Saier MH, Tran CV, Barabote RD. 2006. TCDB: the transporter classification database for membrane transport protein analyses and information. Nucleic Acids Res 34:D181–6. https://doi.org/10.1093/nar/gkj001
160. Graham ED, Heidelberg JF, Tully BJ. 2018. Potential for primary productivity in a globally-distributed bacterial phototroph. ISME J 12:1861–1866. https://doi.org/10.1038/s41396-018-0091-3
161. Mall A. 2023. KEGG-decoder-carbonfixation. GitHub repository. Available from: https://doi.org/https://github.com/achmall/KEGG-decoder-carbonfixation
162. Garber AI, Nealson KH, Okamoto A, McAllister SM, Chan CS, Barco RA, Merino N. 2020. FeGenie: a comprehensive tool for the identification of iron genes and iron gene neighborhoods in genome and metagenome assemblies. Front Microbiol 11:37. https://doi.org/10.3389/fmicb.2020.00037
163. Pal C, Bengtsson-Palme J, Rensing C, Kristiansson E, Larsson DGJ. 2014. BacMet: antibacterial biocide and metal resistance genes database. Nucleic Acids Res 42:D737–43. https://doi.org/10.1093/nar/gkt1252
164. Supek F, Vlahovicek K. 2005. Comparison of codon usage measures and their applicability in prediction of microbial gene expressivity. BMC Bioinformatics 6:182. https://doi.org/10.1186/1471-2105-6-182
165. Fu L, Niu B, Zhu Z, Wu S, Li W. 2012. CD-HIT: accelerated for clustering the next-generation sequencing data. Bioinformatics 28:3150–3152. https://doi.org/10.1093/bioinformatics/bts565
166. Larsson A. 2014. AliView: a fast and lightweight alignment viewer and editor for large datasets. Bioinformatics 30:3276–3278. https://doi.org/10.1093/bioinformatics/btu531
167. Nayfach S, Camargo AP, Schulz F, Eloe-Fadrosh E, Roux S, Kyrpides NC. 2021. CheckV assesses the quality and completeness of metagenome-assembled viral genomes. Nat Biotechnol 39:578–585. https://doi.org/10.1038/s41587-020-00774-7
168. Kieft K, Zhou Z, Anantharaman K. 2020. VIBRANT: automated recovery, annotation and curation of microbial viruses, and evaluation of viral community function from genomic sequences. Microbiome 8:90. https://doi.org/10.1186/s40168-020-00867-0
169. Ren J, Song K, Deng C, Ahlgren NA, Fuhrman JA, Li Y, Xie X, Poplin R, Sun F. 2020. Identifying viruses from metagenomic data using deep learning. Quant Biol 8:64–77. https://doi.org/10.1007/s40484-019-0187-4
170. Roux S, Adriaenssens EM, Dutilh BE, Koonin EV, Kropinski AM, Krupovic M, Kuhn JH, Lavigne R, Brister JR, Varsani A, et al. 2019. Minimum information about an uncultivated virus genome (MIUVIG). Nat Biotechnol 37:29–37. https://doi.org/10.1038/nbt.4306
171. Altschul SF, Gish W, Miller W, Myers EW, Lipman DJ. 1990. Basic local alignment search tool. J Mol Biol 215:403–410. https://doi.org/10.1016/S0022-2836(05)80360-2
172. Paez-Espino D, Eloe-Fadrosh EA, Pavlopoulos GA, Thomas AD, Huntemann M, Mikhailova N, Rubin E, Ivanova NN, Kyrpides NC. 2016. Uncovering earth's virome. Nature 536:425–430. https://doi.org/10.1038/nature19094
173. Lowe TM, Eddy SR. 1997. tRNAscan-SE: a program for improved detection of transfer RNA genes in genomic sequence. Nucleic Acids Res 25:955–964. https://doi.org/10.1093/nar/25.5.955
174. Galiez C, Siebert M, Enault F, Vincent J, Söding J. 2017. WisH: who is the host? predicting prokaryotic hosts from metagenomic phage contigs. Bioinformatics 33:3113–3114. https://doi.org/10.1093/bioinformatics/btx383
175. Gregory AC, Zablocki O, Zayed AA, Howell A, Bolduc B, Sullivan MB. 2020. The gut virome database reveals age-dependent patterns of virome diversity in the human gut. Cell Host Microbe 28:724–740. https://doi.org/10.1016/j.chom.2020.08.003
176. Lu C, Zhang Z, Cai Z, Zhu Z, Qiu Y, Wu A, Jiang T, Zheng H, Peng Y. 2021. Prokaryotic virus host predictor: a gaussian model for host prediction of prokaryotic viruses in metagenomics. BMC Biol 19:5. https://doi.org/10.1186/s12915-020-00938-6